Synthesis, Characterization, Electronic & Redox Properties of 28π, 42π and 56π Thia Porphyrinoids

A Thesis

submitted to

Indian Institute of Science Education and Research Pune in partial fulfilment of the requirements for the Integrated PhD Degree Program

by

Nikita Panchmukhi

Indian Institute of Science Education and Research Pune

Dr. Homi Bhabha Road,

Pashan, Pune 411008, INDIA.

April, 2024

Supervisor: Prof. V. G. Anand

Nikita Panchmukhi (20212010)

Certificate

This is to certify that this dissertation entitled ***'Synthesis, Characterization, Electronic & Redox Properties of 28π, 42π and 56π Thia Porphyrinoids'*** towards the partial fulfilment of the Integrated PhD degree program at the Indian Institute of Science Education and Research, Pune represents study/work carried out by Nikita Panchmukhi at Indian Institute of Science Education and Research under the supervision of V. G. Anand, Professor, Department of Chemistry, during the academic year 2023-2024.

Prof. V. G. Anand

Committee:

Prof. V. G. Anand

Dr. Shabana Khan

This thesis is dedicated to Mom, Dad and Nammy

Declaration

I hereby declare that the matter embodied in the report entitled ***'Synthesis, Characterization, Electronic & Redox Properties of 28π, 42π and 56π Thia Porphyrinoids'*** are the results of the work carried out by me at the Department of Chemistry, Indian Institute of Science Education and Research, Pune, under the supervision of Prof. V. G. Anand and the same has not been submitted elsewhere for any other degree. Wherever others contribute, every effort is made to indicate this clearly, with due reference to the literature and acknowledgement of collaborative research and discussions.

Your Name: Nikita Panchmukhi
(20212010)

Date: 27/03/2024

Table of Contents

List of Tables

Abbreviations

RT	Room Temperature
NMR	Nuclear Magnetic Resonance
MALDI-TOF/TOF	Matrix Assisted Laser Desorption Ionization-Time Of Flight
DDQ	2,3-Dichloro-5,6-dicyano-1,4-benzoquinone
THF	Tetrahydrofuran
DCM	Dichloromethane
DMF	Dimethylformamide
CV	Cyclic Voltammetry
DPV	Differential Pulse Voltammetry
TBAP	Tetrabutylammonium perchlorate
HRMS	High Resolution Mass Spectrometry
UV	Ultraviolet
ESR	Electronic Spin Resonance
NICS	Nucleus Independent Chemical Shift
ACID	Anisotropy Induced Current Density
GIAO	Gauge Independent Atomic Orbital
CSGT	Continuous Set of Gauge Transformation

List of Figures

Schemes

Abstract

Higher analogues of isophlorins with distinct structural and photophysical characteristics have been accomplished by increasing the heterocyclic units in the core modified isophlorin. Herein, we attempted synthesis of thiophene based expanded isophlorins with antiaromatic 4nπ systems containing 28π and 56π electrons and aromatic 4n+2 π systems containing 42π electrons has been described. Apart from their synthesis, structural characterization by MALDI-TOF/TOF, High Resolution Mass Spectroscopy (HRMS) and ^{1}H NMR, Redox Charcterization through UV-Vis absorption studies, Cyclic Voltammetry and Spectroelectrochemistry and Computational Studies (AICD, NICS (0)) have been carried out for all the macrocycles. A reversible two electron oxidation carried out with Meerwein salt, $[Et_3O]^+[SbCl_6]^-$ was observed for all the three macrocycles forming their corresponding dications. Furthermore, solid state analysis were carried out using Single Crystal X-ray diffractometer which revealed their molecular structures.

Acknowledgments

I owe a debt of gratitude to my mentor, Professor V.G. Anand, for giving me the chance to work in his laboratory. His academic guidance, inspiration, and scientific methodology have been invaluable to me as I work on this project. I would want to express my gratitude to Dr. Shabana Khan, a member of my TAC, for her insightful comments during my mid-year presentation and for expanding the potential for more discoveries.

I want to express my appreciation to my mentor Pragati Shukla for all of her help and advice along the way. Being a guide not just inside the lab but even outside the work hours has helped me a lot. I would like to thank my lab mates Dr. Sunita, Dr. Udaya, Vishnu, Markose, Ramesh, Rakesh for their kind help and cooperation thus making the lab a friendly and safe place to work in. Their valuable suggestions have helped me throughout my journey.

I want to express my heartfelt gratitude to Amma, Appa, and Nammy for their unwavering support. I would like to thank Prem Agarwal for being the best person I could have ever asked for. To Shlok, Manasmita and Shrutika for being the other trustworthy people to lean on. These people have constantly supported me, both physically and virtually and that has helped me be a better version of myself.

I am thankful to the technical staff for helping me with instrumentation and timely data collection. My sincere thanks to Prof. Maheswaran Shanmugam, IIT Bombay for recording the EPR measurements. My master's thesis would be incomplete without the support from these people.

Lastly, I am grateful to myself for having endured throughout my master's journey. This journey has not only taught me patience and persistence but also obedience, commitment and honesty towards my work. I am beyond grateful to all the other people whose names might have been unintentionally missed out. Also, I would like to thank all those of you who are going to read my master's thesis. Onwards and upwards!

~Nikita Panchmukhi

CHAPTER-1. INTRODUCTION

π-conjugated systems have been explored extensively for their photo-physical properties, synthetic challenges, optoelectronic properties, etc. These structures belong to two categories: linear and macrocyclic. The π-electron delocalization in a circular conjugated network enables new electrical features, including ring currents for planar molecules. Hückel first used the term "aromatic" for describing conjugated planar molecules with (4n+2)π electrons [1]. Systems become “non-aromatic” when conjugated molecules lose their planarity, which reduces the effects of ring currents. Ronald Breslow first coined the term "anti-aromatic" to describe planar compounds with 4nπ electrons that have opposite ring current effects and less stability than their aromatic congeners [2]. For similar reasons, anti-aromatic systems are moderately less studied.

Owing to the π-electron delocalization and ring current effects, a class of molecules called “annulenes” exhibit aromaticity and have been extensively studied by various groups. A series of annulenes consisting of 12π to 18π electrons were first synthesized by Sondheimer and coworkers to check for aromaticity.[3] They were found to obey Hückel’s (4n+2)π rule. However, higher analogues consisting of 22π electrons or more could not be studied due to conformational flexibility and solubility issues in common organic solvents.[4] On the other hand, anti-aromaticity was considered to destabilize π electron delocalization.

While discovering the synthetic pathway of Vit B_{12}, Woodward identified the formation of an 18π pyrrole containing macrocycle termed as “porphyrin” via oxidizing an unstable antiaromatic 20π intermediate, termed as “isophlorin”.[5] Porphyrin is an 18π aromatic aza-annulene, which comprises regularly arranged four methine carbons and four pyrroles. Porphyrins and their higher analogues serve as one of the best examples of extended π conjugation. Being an aromatic molecule, it exhibits diatropic ring current effects, evident from ^{1}H NMR spectroscopy (upfield shift of -NH protons located interior and the downfield shift of peripheral protons). However, the porphyrin like macrocycles were considered as aza annulenes due to the interconversion of amine to its imine form along the conjugation. In recent years, several unnatural structural analogs of porphyrin such as isophlorin [6],

core-modified porphyrin [7], and ring expanded porphyrins [8], etc have been studied by modifying its structure. There had been constant efforts to isolate the unstable 20π isophlorin.

1.1 ISOPHLORIN

Isophlorin is a non-natural '20π anti-aromatic' macrocycle. It is an amalgamation of porphyrin and annulene structural elements. Vogel identified it as a "cyclobutadiene analogue" owing to its 4nπ planar conformation.[9] Woodward postulated it as a likely unstable intermediary in the synthesis of chlorophyll in 1960. It was hypothesized as a product formed by four-electron oxidation of porphyrinogen, **I.1**, that was further synthesized by condensing pyrrole and aldehyde under acidic conditions, obeying Rothemund type condensation. It is anticipated that the process of further oxidizing porphyrinogen to porphyrin, I.3 occurs in two steps **(Figure 1)**. The porphyrinogen is first oxidized by four electrons to become the unstable 20π Isophlorin **(I.2)** which further undergoes oxidation by two electrons forming the stable18π Porphyrin **(I.3)**.

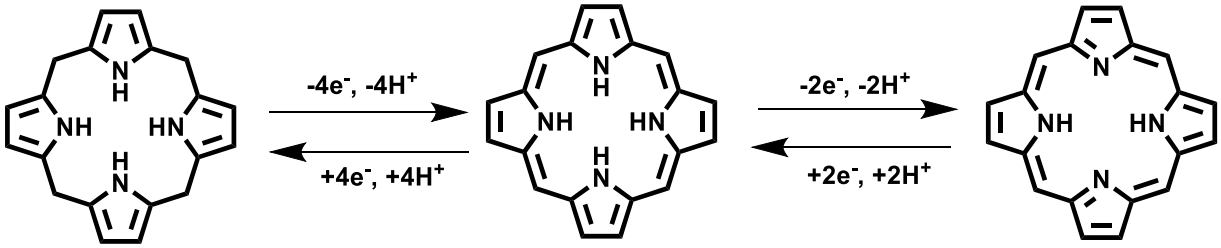

Figure-1: Proton coupled electron transfer of Porphyrinogen, **I.1**, Isophlorin, **I.2**, and Porphyrin, **I.3**.

Porphyrin (18π) is a heteroannulene, with two sp^2 hybridized nitrogens. It is planar and obeys Hückel's rule of aromaticity.[10] On the other hand, isophlorin (20π, anti-aromatic) is devoid of nitrogen's contribution in sp^2 hybridisation, with the π-electron delocalization occurring only through the periphery.[11] The steric repulsion from the four hydrogens in the center induces the isophlorin to deviate away from planarity. To overcome this steric

hindrance, Vogel *et al* synthesized a macrocycle by substituting pyrrole rings of porphyrin entirely by thiophene/furan/selenophene units.[12] This modification yielded stable, neutral 20π electron conjugated system. However, they were unstable in ambient conditions and underwent a rapid oxidation by two electrons to form an 18π porphyrin dication.[13] Several attempts were made in order to stabilize these 4nπ systems; in 2005, Vaid *et al* reported silicon (IV) Isophlorin **(2).**[14] This compound was found to be sensitive to ambient conditions and distort upon complexation. Chen *et al* developed a tetra pyrrole Isophlorin in 2007 by substituting electron-withdrawing trifluoromethyl substituents in place of β hydrogens, thereby enhancing its stability **(3)**.[15] **(Figure-2)**

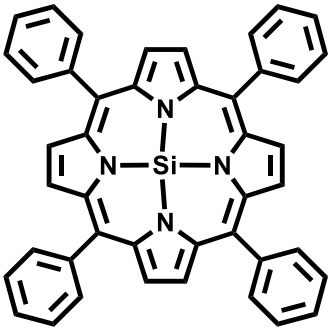

2

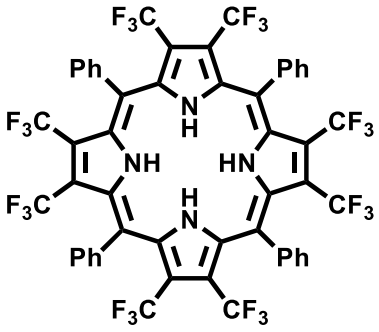

3

Figure-2: Earlier attempts of achieving 20π tetrapyrrolic isophlorins.

1.2 CORE-MODIFIED ISOPHLORINS

The isophlorin-porphyrin redox system is favored towards the 18π porphyrin system because of its Hückel type aromaticity. The removal of two protons from two amines, renders them into imines, favoring 18π delocalized pathway. Replacement of 2° N with 3° N partially prevents the deprotonation process. Divalent chalcogens are an appropriate substitute to 3° N as they retain similar structural as well electronic properties. Vogel and co-workers synthesized tetrathia/tertraoxa/tetraselena-porphyrin dications with a carbon bridge connecting the heterocyclic units.[16] The tetraoxaisophlorin **(4)** was stable only at low temperature (-78°C). Another significant discovery was the neutral N, N', N", N'"-

tetramethylisophlorin having octa-ethyl substitution on the periphery **(5)** [17]. It was discovered to be quite stable in the presence of air, in contrast to the more reactive tetraoxaisophlorin. **(Figure-3)**

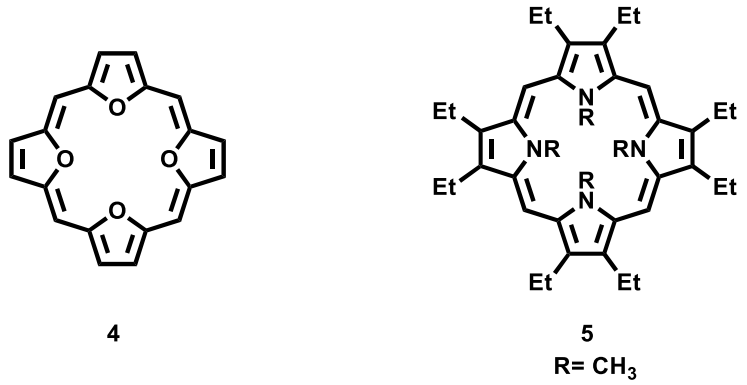

Figure-3: Core-modified isophlorins.

The substitution on the meso-carbons by robust electron-withdrawing pentafluorophenyl groups created stable tetraoxa **(6)** and dioxa dithia **(7)** 20π isophlorins, as described by Reddy and Anand in 2008 [18]. Their distinct ^{1}H NMR spectra displayed a strong effect of paratropic ring current. These compounds are the first stable 4nπ systems that can withstand powerful oxidizing agents like perchloric acid without being oxidized to 18π aromatic dications. Tetrathia isophlorin **(8)** was created using a method akin to this one, called the "acid-catalyzed cyclic condensation of 2-(1-hydroxy-1-pentafluorophenylmethyl) thiophene." The analysis from Single-Crystal X-ray diffraction clearly showed its non-planar geometry, owing to the lack of strong effects of paratropic ring current in its ^{1}H NMR spectra.[19] **(Figure-4)**

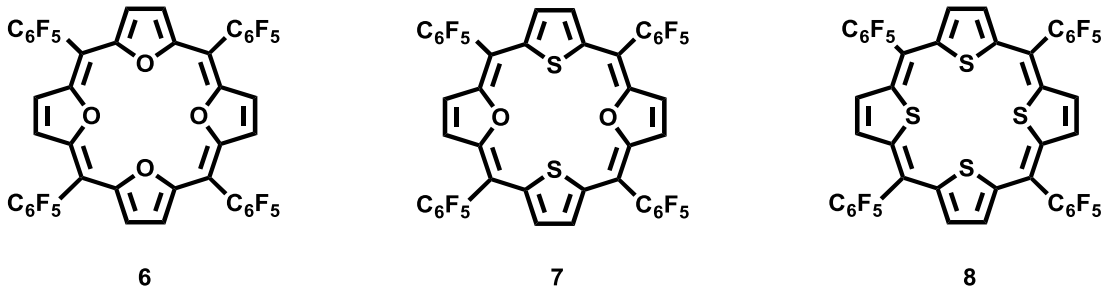

Figure-4: Stable core-modified, meso-aryl substituted 20π isophlorins.

1.3 EXPANDED CORE MODIFIED ISOPHLORINS

Many groups tried to synthesize macrocycles consisting of more than 20π electrons. Increase in π-electron conjugation was achieved by either enhancing the carbon bridges connecting the heterocyclic units **(9)** or by enhancing the heterocyclic units **(11) (Figure-5)**.[20] The electronic properties of core-modified isophlorins were tuned by incorporating such modifications.

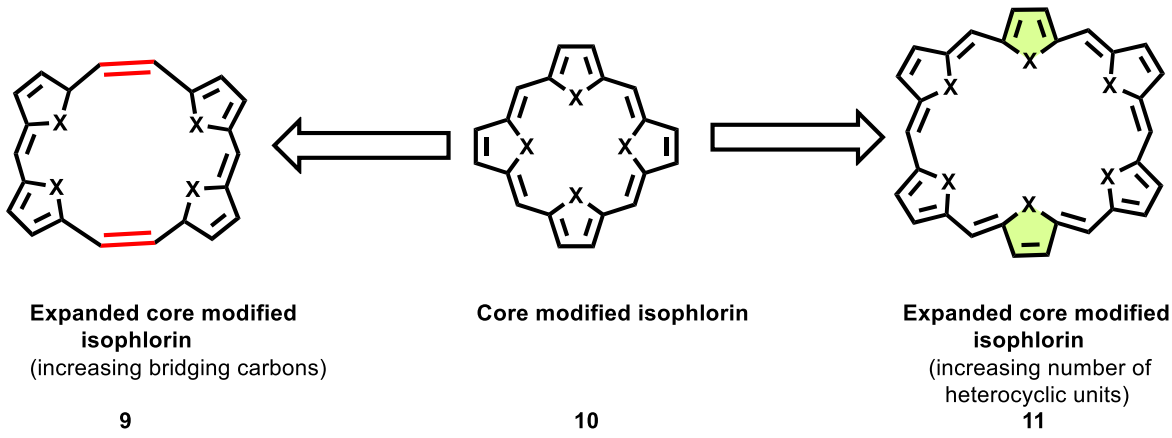

Expanded core modified isophlorin
(increasing bridging carbons)

9

Core modified isophlorin

10

Expanded core modified isophlorin
(increasing number of heterocyclic units)

11

Figure-5: Expansion of Core-Modified Isophlorins.

The first expanded Sapphyrin **(12)**, discovered by R. B. Woodward was identified as a pentapyrrolic macrocycle.[21] Osuka *et al* synthesized a range of enlarged porphyrins bearing five to twelve pyrroles connected by an identical number of meso-carbon bridges. All these macrocycles showed red-shifted absorbance and color change in their respective solutions due to the enhanced π-electron conjugation.[22] **(Figure-6)**

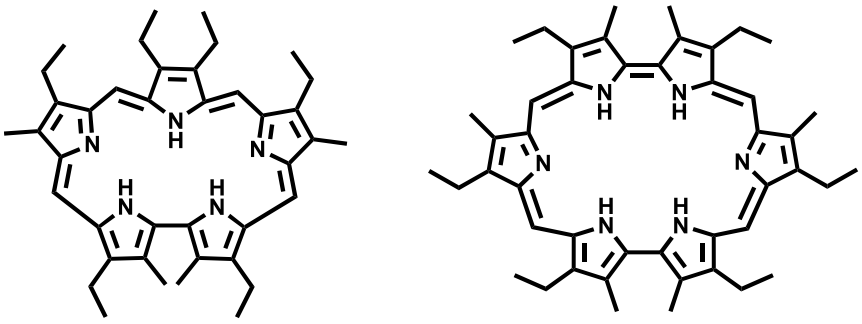

12

13

Figure-6: All-aza expanded porphyrins.

1.4 RUBYRIN AND IT'S HIGHER ANALOGUES

Sessler and colleagues reported a higher congener of Sapphyrin, called Rubyrin **(13)**, with six pyrrole units in 1991. This was achieved by condensing the acetoxy-activated pyrrole and bipyrrole under acidic conditions, and further a [4] + [2] MacDonald-type acid-catalyzed oxidative condensation using the easily accessible diformyl bipyrrole.[23] It was reported to be a Huckel's aromatic system having 26π (4n+2) electrons along its conjugated pathway. Its aromaticity was confirmed through ^{1}H NMR spectrum, with the inner pyrrolic protons shielded and resonating in the upfield region and the outer protons deshielded and resonating in the downfield region.

In 1992, Sessler *et al* discovered a new category of hexapyrrolic expanded porphyrins, called Rosarin.[24] Meso-phenyl substituted hexaphyrin, was first reported by David Dolphin in 1997 through a 3+3 type condensation between 5,10-diphenyltripyrrane and benzaldehyde, followed by oxidation using chloranil, giving a blue colored 26π hexaphyrin.[25] Cavaleiro *et al* reported a different class of hexaphyrins with meso-pentafluorophenyl substitution in 1999.[26] Two spots, violet **(14)** and blue **(15)**, corresponding to the same R_f value and same *m/z* mass were observed in Thin Layer Chromatography. Addition of DDQ converted the blue-colored compound to violet while addition of $TsNHNH_2$ converted the violet-colored compound to blue. The blue-colored compound was later attributed to the 28π system while the violet-colored compound corresponded to the 26π system respectively. Later on, ^{1}H-NMR studies confirmed the aromatic and the anti-aromatic nature of **(14)** and **(15)** respectively. **(Figure-7)**

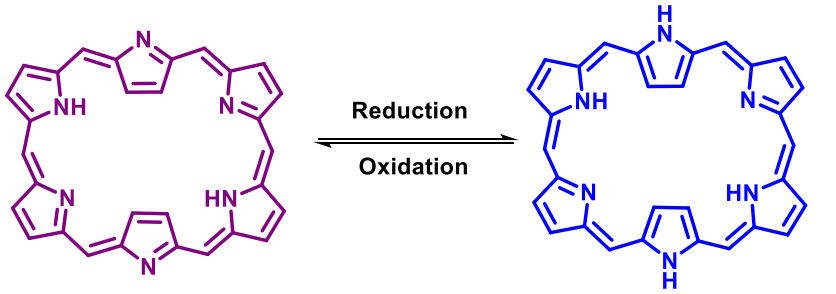

[26]hexaphyrin(1.1.1.1.1.1) **(14)**

[28]hexaphyrin(1.1.1.1.1.1) **(15)**

Figure-7: Redox chemistry of Hexaphyrin.

Expanded porphyrins were relatively less studied owing to their unusually higher reactivity, thereby contributing to decreased stability. Setsune *et al* reported a 48π dodecaphyrin by employing Rothemund type condensation of a bulky-group substituted aldehyde and 2,2'-bipyrrole with a weak acid. [27] A series of expanded porphyrins, including a 26π hexaphyrin and a 40π nonaphyrin, having meso-aryl substitution were reported by Osuka and colleagues in 2001. [28] The given macrocycles were synthesized via an acid-catalyzed coupling of pyrrole and pentafluorobenzaldehyde and further oxidation by DDQ. **(Figure-8)** Amongst the isolated macrocycles was a 42π aromatic nonaphyrin-TFA complex, that adopted a twisted helical conformation. This accounts for one of the first examples of an isolated nonaphyrin. **(Figure-9)**

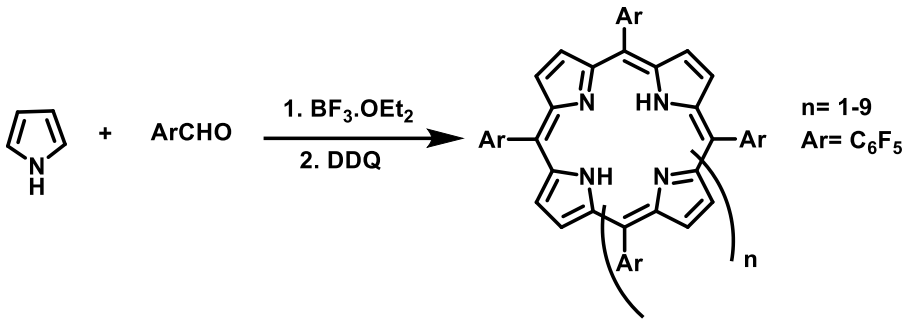

Figure-8: Synthesis of expanded porphyrins having meso-aryl substitution.

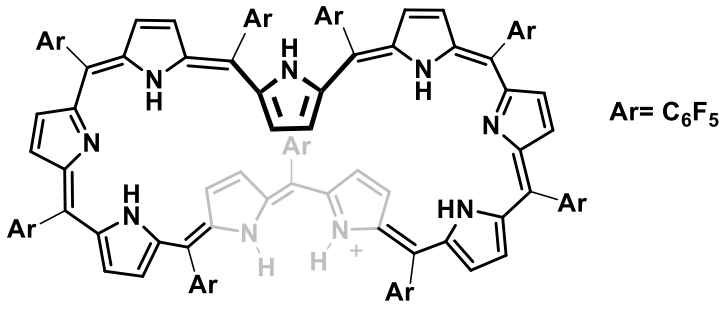

Figure-9: Twisted helical conformation of 42π nonaphyrin-TFA complex.

Years later, the synthesis of meso-aryl rubyrin and higher porphyrinoids was reported by Sessler and Osuka's groups. Oxidative coupling of tripyrrane under acid-catalyzed conditions followed by oxidation using chloranil, maintaining reflux conditions, yielded 26π rubyrin (1.1.0.1.1.0), 38π nonaphyrin (1.1.0.1.1.0.1.1.0), 52π dodecaphyrin

(1.1.0.1.1.0.1.1.0.1.1.0), and 62π pentadecaphyrin (1.1.0.1.1.0.1.1.0.1.1.0.1.1.0). [29] **(Figure-10)**

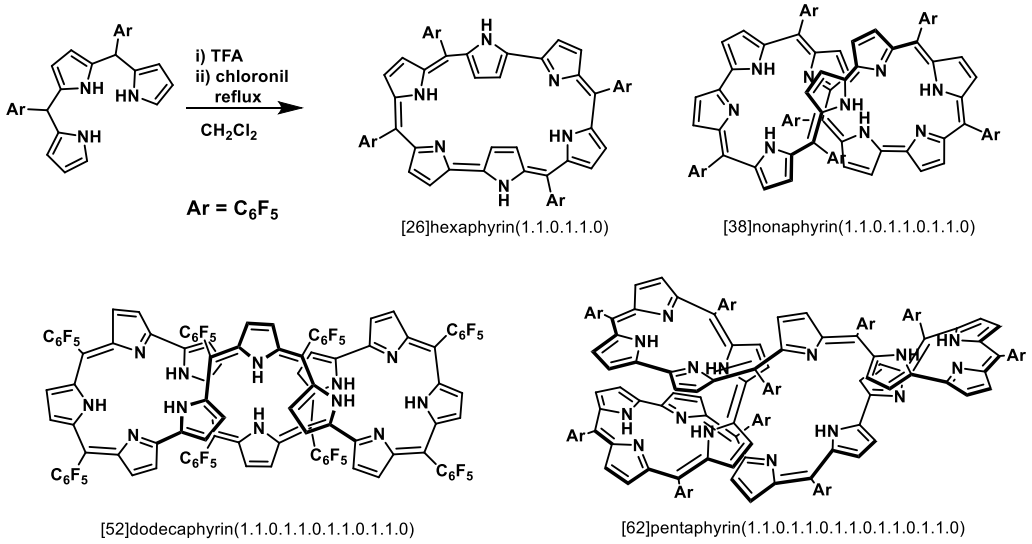

Figure-10: All-aza pentaflurophenyl substituted expanded isophlorins.

Following the synthesis of all-aza higher porphyrinoids, Chandrashekhar and colleagues discovered and reported a range of meso-aryl substituted, core-modified rubyrins and dodecaphyrins via condensation of terthiophene diol and tripyrranes under acidic conditions. [30] **(Figure-11)**

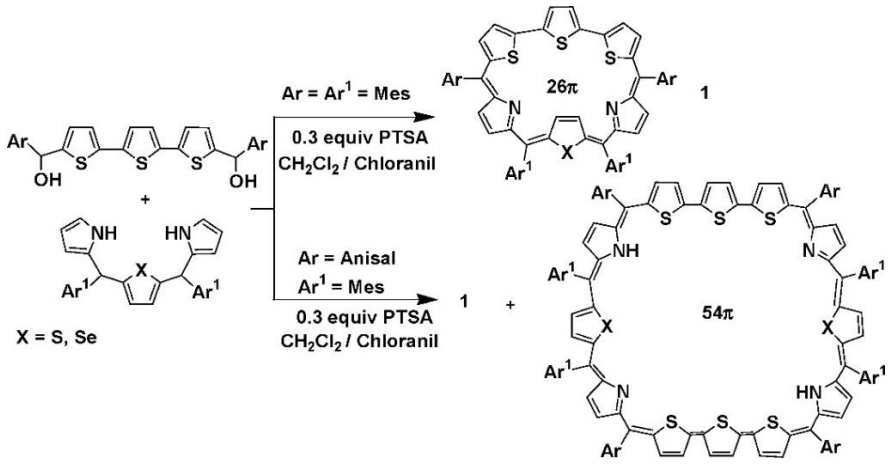

Figure-11: Meso-aryl, core-modified rubyrin and its higher analogues.

Several years later, Setsune *et al* reported a thienylene-containing nonaphyrin **(16)** which adopted a triangular geometry. It consisted of three thienylene units that were inverted and hence pointing away from the macrocyclic core. [31]

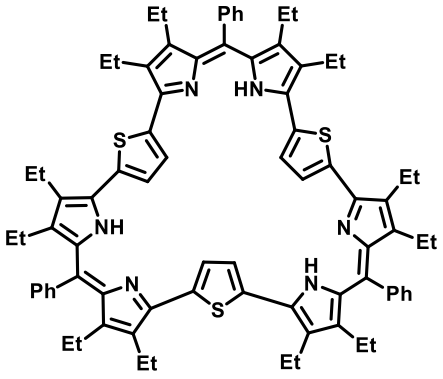

(16)

Recently, in 2022, a series of cyclooligothiophenes were reported by Anand and co-workers. A range of isophlorinoids bearing four to sixteen thiophene rings were prepared through modified Rothemund–Lindsey condensation between thiophene and pentafluorobenzaldehyde, as observed from the reaction mixture's MALDI-TOF/TOF mass spectrum. [32] **(Figure-12)**

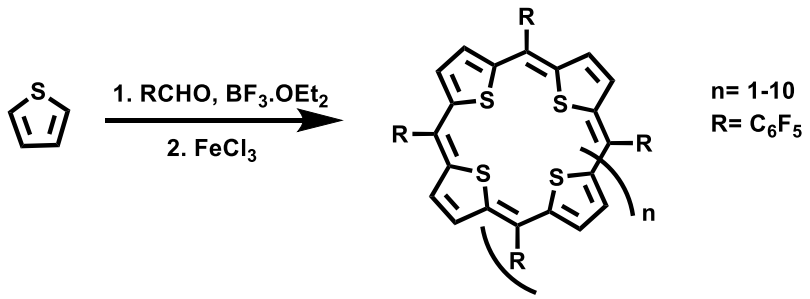

Figure-12: Synthesis of cyclooligothiophenes having meso-aryl substitution.

However, the synthesis of meso-aryl rubyrins and higher homologues, with all the pyrroles replaced with thiophenes hasn't been much discovered. The aim of the thesis is to explore the synthesis, characterization, and redox properties of all-thia [28π] hexaphyrin (1.1.0.1.1.0), [42π] nonaphyrin (1.1.0.1.1.0.1.1.0), and [56π] dodecaphyrin (1.1.0.1.1.0.1.1.0.1.1.0) having pentafluorophenyl substitution on the meso carbons.

CHAPTER-2. METHODS AND MATERIALS

2.1 GENERAL INFORMATION

A two necked round bottom (RB) flask was used for carrying out all the reactions under nitrogen atmosphere. In addition, oxidation using DDQ was carried out in open atmosphere. Dichloromethane was dried prior to use with phosphorous pentoxide (P_2O_5). Sigma Aldrich, Alfa-Aesar and TCI chemicals were purchased and used for the reactions. Aluminum oxide (basic) was used from Merck for column chromatography. A size exclusion column was performed in THF bought from Spectrochem.

2.2 ANALYTICAL INFORMATION

Column chromatography was accomplished using silica gel (100-200 mesh) in glass columns. Either JEOL 400 MHz or Bruker 400 MHz or Bruker 500 MHz spectrometer were used for recording the ^{1}H-NMR spectra. A delta-scale (in ppm) relative to $(CH3)_2CO$ (δ = 2.05 ppm) or CD_2Cl_2 (δ = 5.51 ppm) or $CDCl_3$ (δ = 7.26 ppm) or Tetrahydrofuran-d8 (δ = 3.58 and 1.73 ppm) was used for reporting the chemical shifts. A Shimadzu UV-3600 spectrophotometer and a quartz cuvette of path length 1 cm were used for recording the electronic spectra. A WATERS G2 Synapt Mass Spectrometer were used for recording High Resolution Mass spectra. Data for Single-Crystal diffraction investigation were obtained at 100K using graphite-monochromated Mo Kα radiation (λ = 0.71073 Å) and a BRUKER KAPPA APEX II CCD Duo diffractometer (run at 1500 W power: 50 kV, 30 mA). The analysis of crystal structure was done with APEX2 and refinement was done in SHELXL-97 [33], and WINGX. [34] Using the PLATON software package's SQUEEZE feature, scattering contributions from the solvent molecules disordered in the crystal were eliminated. [35] On a BAS electrochemical system, Differential Pulse Voltammetry (DPV) and Cyclic Voltammetry (CV) measurements were measured using a traditional three-electrode cell (Glassy Carbon (Working Electrode), a Platinum Wire (Counter Electrode), and Saturated Hg/Hg+ (Reference Electrode)) in dry CH_2Cl_2 with 0.1 M tetrabutylammonium perchlorate (TBAP) serving as the supporting electrolyte. An inert argon atmosphere was ensured for all the measurements. The final results were calibrated with the ferrocene/ferrocenium couple.

2.3. SYNTHETIC PROCEDURES

2.3.1 (2,5-diformylthiophene)

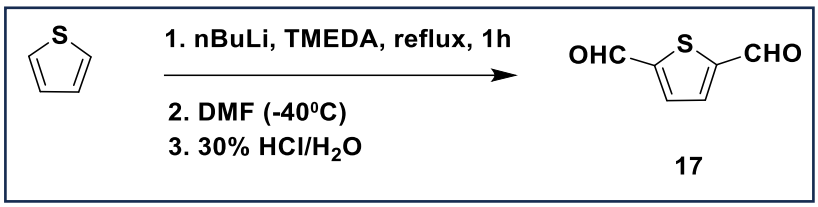

Scheme-1: Synthesis of 2,5-diformylthiophene **(17).**

A hexane solution of nBuLi (2.3 equiv, 2.5M) (21.87 mL, 54.67 mmol) was added to a solution of TMEDA (2.3 equiv) (8.20 mL, 54.67 mmol) in hexane (40 mL) at -78°C followed by addition of thiophene (1 equiv) (1.90 mL, 23.77 mmol). A temperature of 50°C was maintained for the reaction mixture and the conversion to dialdehyde was completed under reflux for 45 minutes. Hexane was added to redissolve the precipitate and the solution's temperature was decreased to -40°C. Excess DMF (5 equiv) (9.20 mL, 118.67 mmol) was added very slowly. The reaction set-up's temperature was unhurriedly increased to RT and allowed to stir for 30 minutes. A 30% HCl/water solution was used to quench the reaction mixture and the aldehyde was separated during the hydrolysis. To neutralize excess HCl, saturated $NaHCO_3$ was added until a pH 6 was obtained for the aqueous layer. Ethyl acetate (7x50 mL) was used to collect the organic layer which was further subjected to brine wash and finally dried over Na_2SO_4. Column chromatography was used to further purify the compound after the solvent evaporation under low pressure to get a pale-yellow solid **(17)** with 15% EtOAc/Hexane. Yield= 64%. **(Scheme-1)**

^{1}H NMR (400 MHz, $CDCl_3$, 298 K): d= 10.04 (s, 2H), 7.85 (s, 2H). **(Figure-13) HRMS** (ESI) *m/z* calculated for $C_6H_4O_2S$ $(M+Na)^+$: 162.9798 , Observed :163.0396. **(Figure-A.1)**

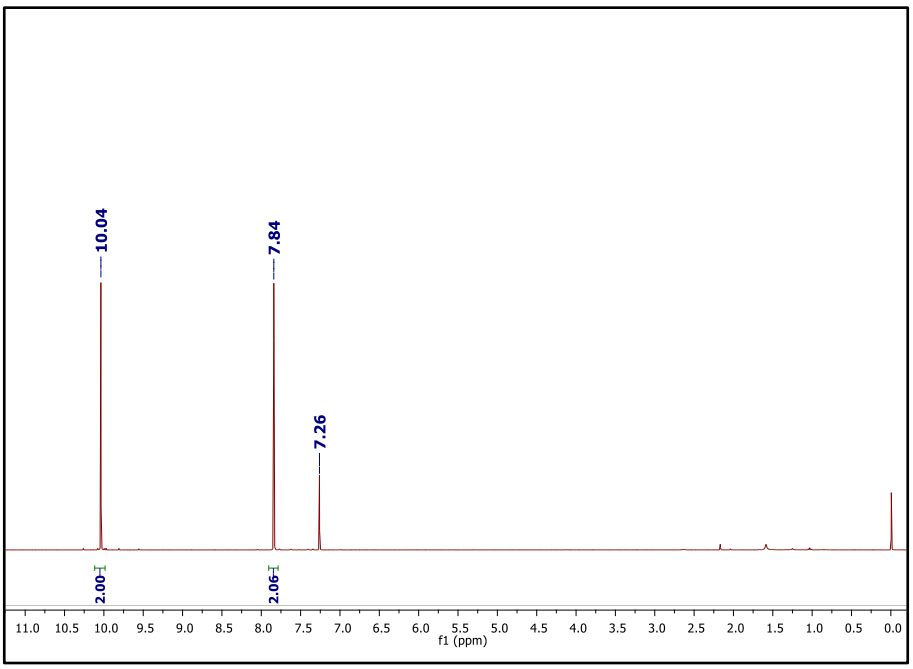

Figure-13: ^{1}H NMR spectrum of **17** in $CDCl_3$ at 298K.

2.3.2 (2,5-bis(pentafluorophenylhydroxymethyl)thiophene)

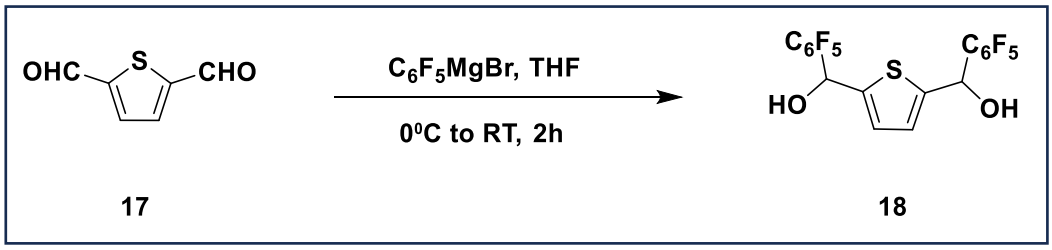

Scheme-2: Synthesis of 2,5-bis(pentafluorophenylhydroxymethyl)thiophene **(18).**

In a 50mL two necked RB equipped with condenser and under N_2 atmosphere, Mg (2.4 equiv) (416.19 mg, 17.12 mmol) was added along with a catalytic amount of I_2 in 15 mL dry THF. The addition of 2-Bromo-2,3,4,5,6-pentafluorobenzene (2.2 equiv) (1.96 mL, 15.70 mmol) was followed by stirring for 1 hour. The grey colored solution indicates the formation of RMgX (Grignard reagent). Then, 2,5-diformylthiophene **(17)** (1 equiv) (1g, 7.13 mmol) in 10-15 mL dry THF was gradually added to the freshly prepared RMgX

solution under N_2 atmosphere. Further stirring of the solution was carried out for 3 hours under inert conditions. A saturated solution of NH_4Cl was then added to quench the reaction mixture. Ethyl acetate (7x50 mL) was used to collect the organic layer which was further subjected to brine wash and finally dried over Na_2SO_4. Column chromatography was used to further purify the chemical after the low-pressure evaporation of solvent to get a white solid **(18)** with 15% EtOAc/Hexane. Yield= 80%. **(Scheme-2)**

^{1}H NMR (400 MHz, $CDCl_3$, 298 K) δ = 6.77 (s, 2H), 6.33 (d, *J* = 7.9 Hz, 2H), 2.84 (d, *J* = 8.4 Hz, 2H). **(Figure-14) HRMS** (ESI) *m/z* calculated for $C_{18}H_6F_{10}O_2S$ $(M+Na)^+$: 498.9826, Observed: 499.0184. **(Figure-A.2)**

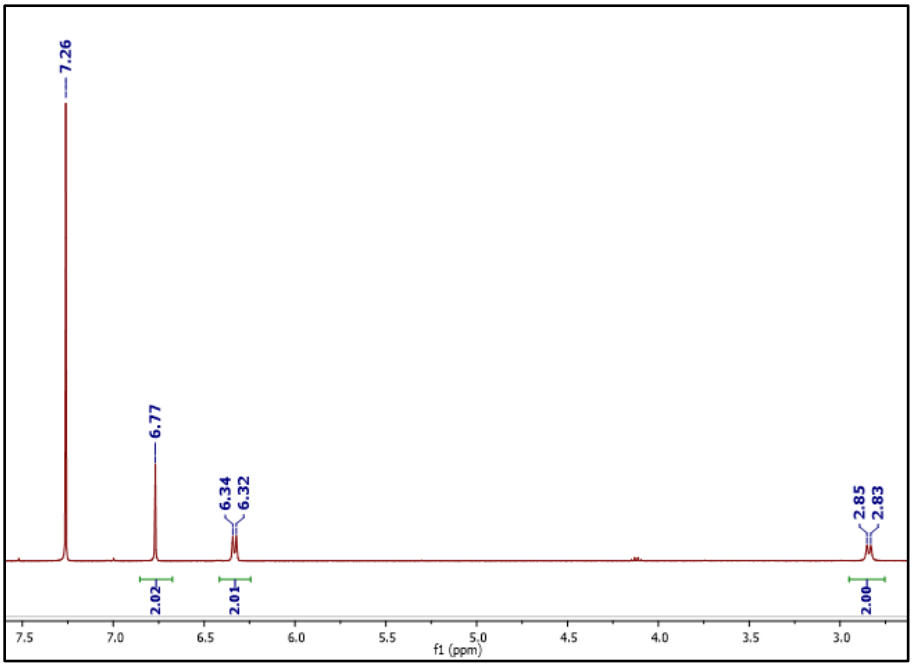

Figure-14: ^{1}H NMR spectrum of **18** in $CDCl_3$ at 298K.

2.3.3 (2,2'-bithiophene)

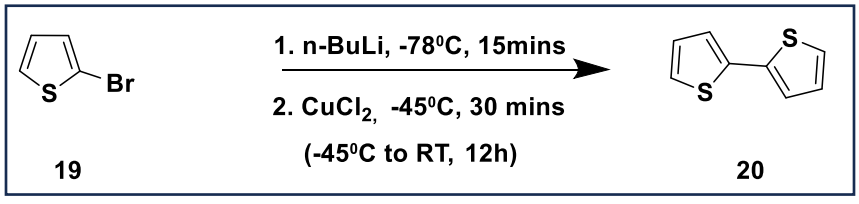

Scheme-3: Synthesis of 2,2'-bithiophene **(20).**

To the stirred solution of 2-bromothiophene, **19**, (1 equiv) (5.94 mL, 61.34 mmol), n-BuLi (1.2 equiv, 1.6M in hexane) (38.34 mL, 61.34 mmol) was added under a very low temperature of -78°C for 30 minutes. The temperature of the reaction mixture was kept undisturbed for 15 minutes, then warmed to -55°C and $CuCl_2$ (1 equiv) (8.25g, 61.34 mmol) was added by portions. The mixture was then stirred at -45°C for one hour and finally overnight at RT. Saturated NH_4Cl (100 mL) was added to quench the reaction mixture. The organic layer was decanted, the H_2O layer filtered. The organic residue was washed with Et_2O and dried over Na_2SO_4. Column chromatographic purification with hexane as eluent was employed after low-pressure solvent evaporation to yield, **20**, as a green solid. Yield: 70%. **(Scheme-3)**

^{1}H NMR (400 MHz, $CDCl_3$, 298 K): δ= 7.17 – 7.14 (m, 2H), 7.14 – 7.12 (m, 2H), 6.96 (dd, *J* = 5.0, 3.7 Hz, 2H). **(Figure-15) HRMS** (ESI) *m/z* calculated for $C_8H_6S_2$ $(M+H)^+$: 166.9911, Observed: 166.9994. **(Figure-A.3)**

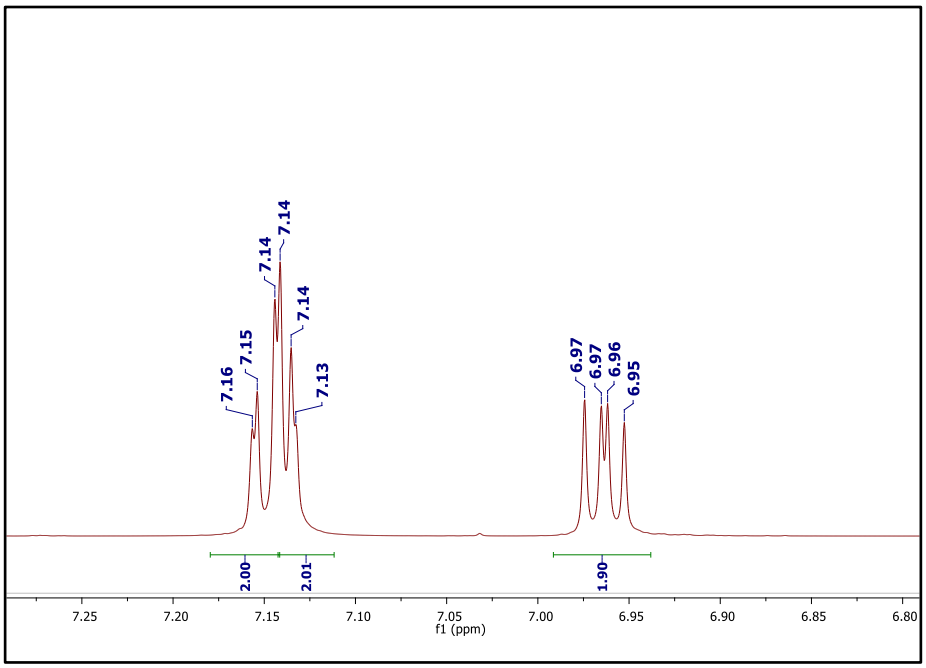

Figure-15: ^{1}H NMR spectrum of **20** in $CDCl_3$ at 298K.

2.3.4 Synthesis of macrocycles

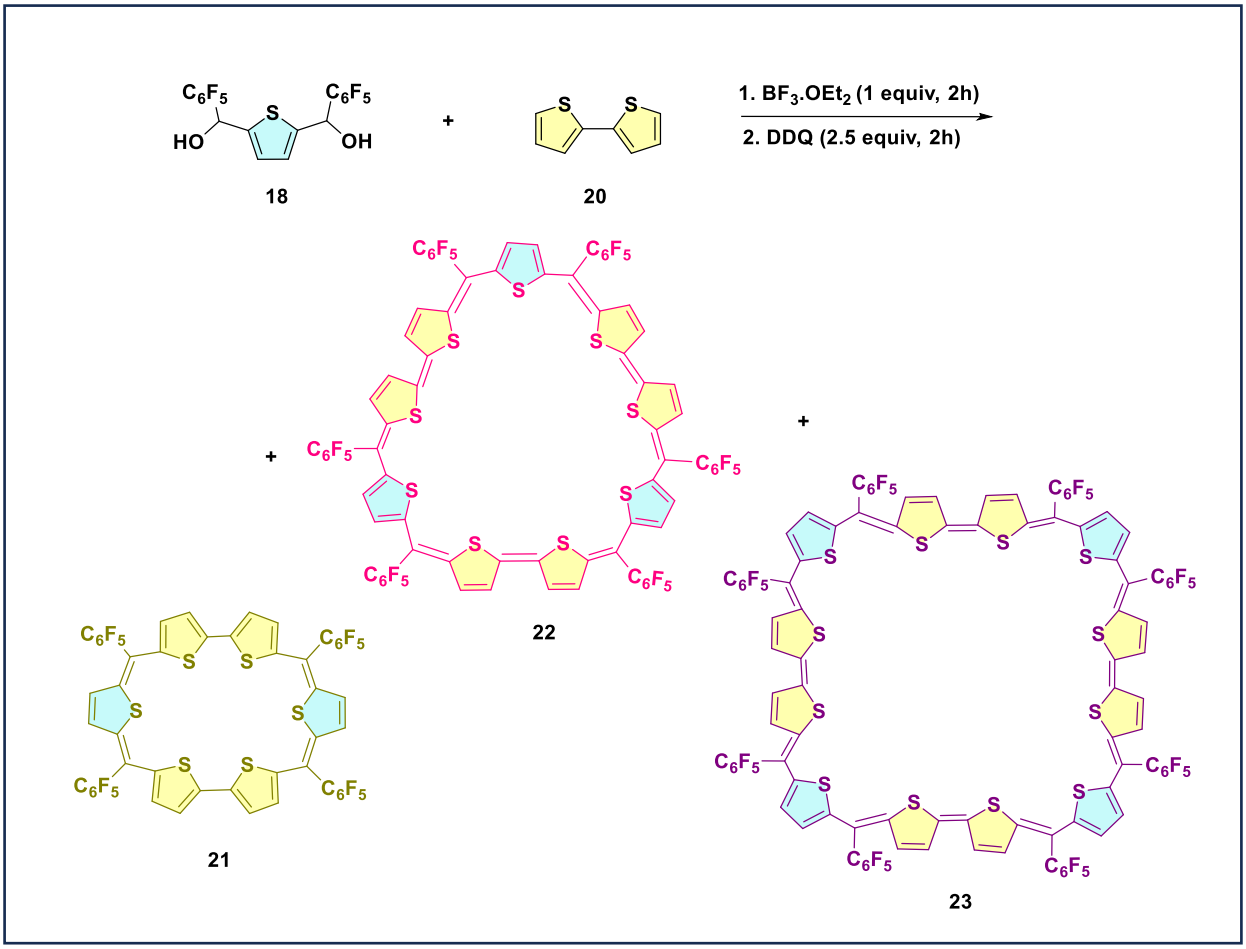

Scheme-4: Synthesis of 28π **(21),** 42π **(22)** and 56π **(23)** via acid-catalyzed condensation and open-air oxidation.

25 mL of dry dichloromethane was used to dissolve an equimolar concentration of bithiophene, **20**, (1 equiv) (34.91 mg, 209.96 μmol), and the diol, **18**, (1 equiv) (100 mg, 209.96 μmol), which were then perched with nitrogen gas for ten minutes. The stirring of reaction mixture after the addition of a catalytic amount of $BF_3.OEt_2$ (1 equiv) (25 mL, 209.96 mmol) was carried out for two hours under inert atmosphere. Later, open-air oxidation of the reaction mixture was carried out with DDQ (2.5 equiv) (119.15 mg, 524.89 μmol) and stirred for an additional two hours. **(Scheme-4).** A short basic alumina column was used to purify the mixture using 100% DCM as the eluent. Following the low-pressure evaporation of solvent, the mixture was subjected to basic-alumina column chromatographic purification using CH_2Cl_2/Hexane as eluent. The given reaction mixture

was finally purified by size-exclusion column chromatography in THF. A pale-yellow band as **21** in 1.3% yield, a pink colored band was identified as **22** in 2% yield and a dark violet band as **23** in 1.5% yield respectively.

21: **^{1}H NMR** (400 MHz, $CDCl_3$, 298 K): δ = 5.44 (d, *J* = 4.2 Hz, 4H), 4.93 (d, *J* = 4.1 Hz, 4H), 4.74 (s, 4H) **22**: **^{1}H NMR** (400 MHz, $CDCl_3$, 298 K): δ = 7.03 (d, *J* = 4.1 Hz, 6H), 6.80 (d, *J* = 4.1 Hz, 6H), 6.73 (s, 6H) **23**: **^{1}H NMR** (400 MHz, $CDCl_3$, 298 K): δ = 7.12 (d, *J* = 4.1 Hz, 8H), 6.82 (d, *J* = 4.1 Hz, 8H), 6.40 (s, 8H).

2.3.5 Synthesis of Dications of 21, 22 and 23

To the stirred solution of **21** in anhydrous dichloromethane, Meerwein's salt, $[Et_3O]^+[SbCl_6]^-$ was added under nitrogen atmosphere at 0^0C. Meerwein's salt is known to oxidize the π-conjugated systems by one-electron. **(Scheme-5)** The pale yellow color solution immediately turns pink. After stirring the resultant solution for one hour, it was then poured to diethyl ether (20 mL) at -78^0C. The solution was kept undisturbed for one hour and then good quality single crystals were grown in acetonitrile. A similar procedure was followed to yield **$[22]^{2+}$** and **$[23]^{2+}$** respectively. The pink color of **(22)** immediately turned blue while the violet color of **(23)** turned pink respectively. **(Scheme-6)**

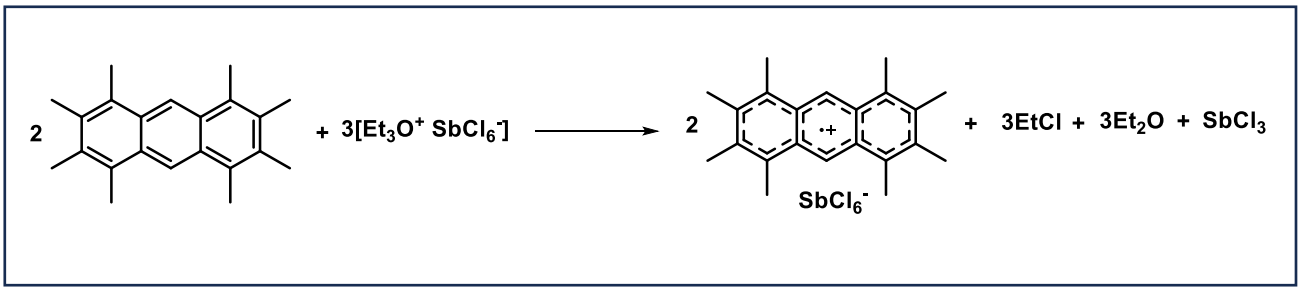

Scheme-5: Illustrative example of oxidation with $[Et_3O]^+[SbCl_6]^-$ (Meerwein's Salt).

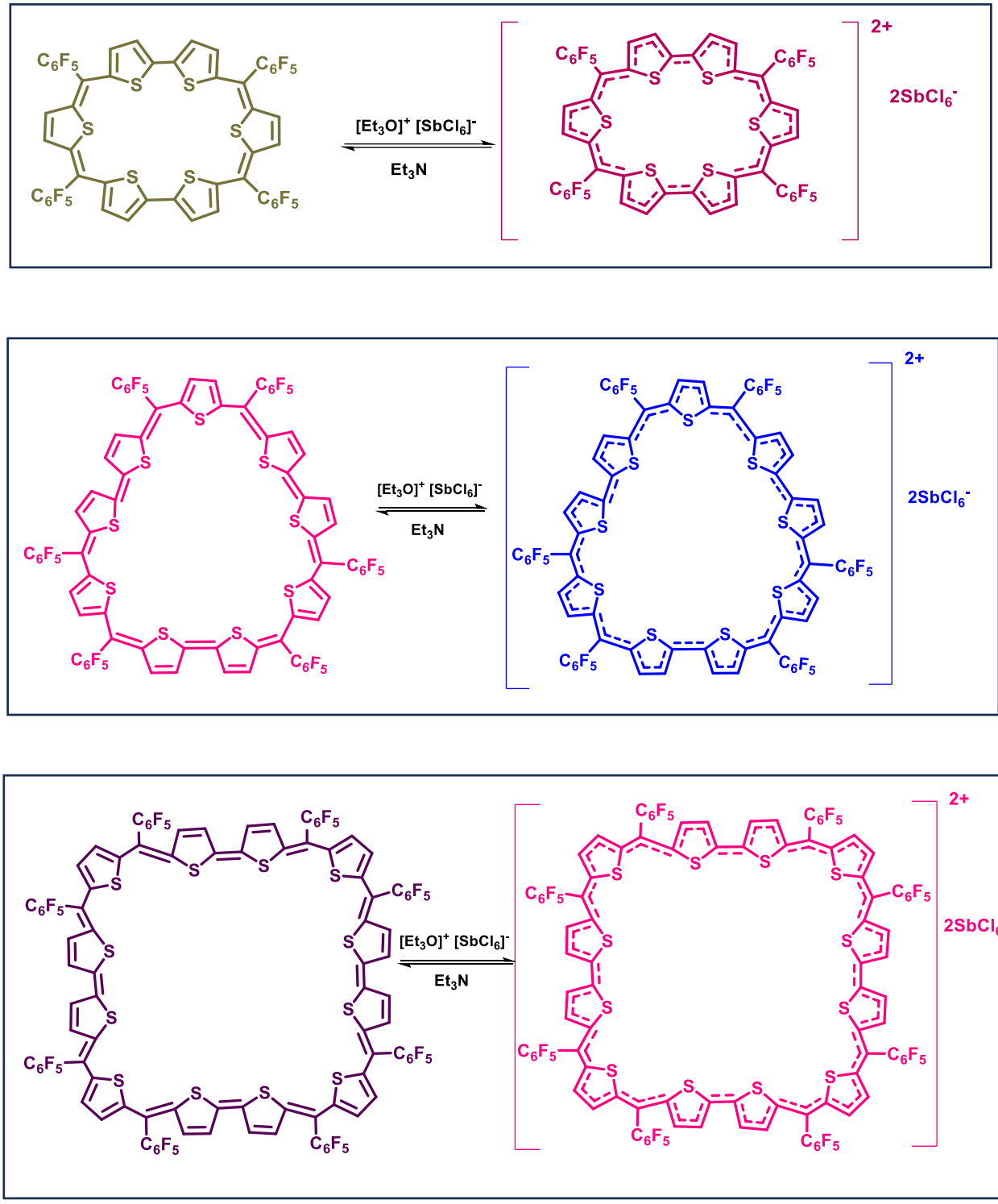

Scheme-6: Synthesis of the corresponding dications of **(21), (22)** and **(23).**

CHAPTER-3. RESULTS AND DISCUSSIONS

3.1 HIGH RESOLUTION MASS SPECTROSCOPY

High Resolution Mass Spectroscopy (HRMS) (ESI) analysis confirmed the composition of the given macrocycles. **21** displayed *m/z* value of 1207.8944, corresponding to $C_{52}H_{12}F_{20}S_6$ (1207.8944) along with its *m/2* mass **(Figure-16)**. **22** and **23** displayed *m/z* value of 1811.8518 corresponding to $C_{78}H_{18}F_{30}S_9$ (1811.8416) **(Figure-17)** and 2417.7981 corresponding to $C_{104}H_{24}F_{40}S_{12}$ (2415.7888) **(Figure-18)** along with their *m/2* masses respectively.

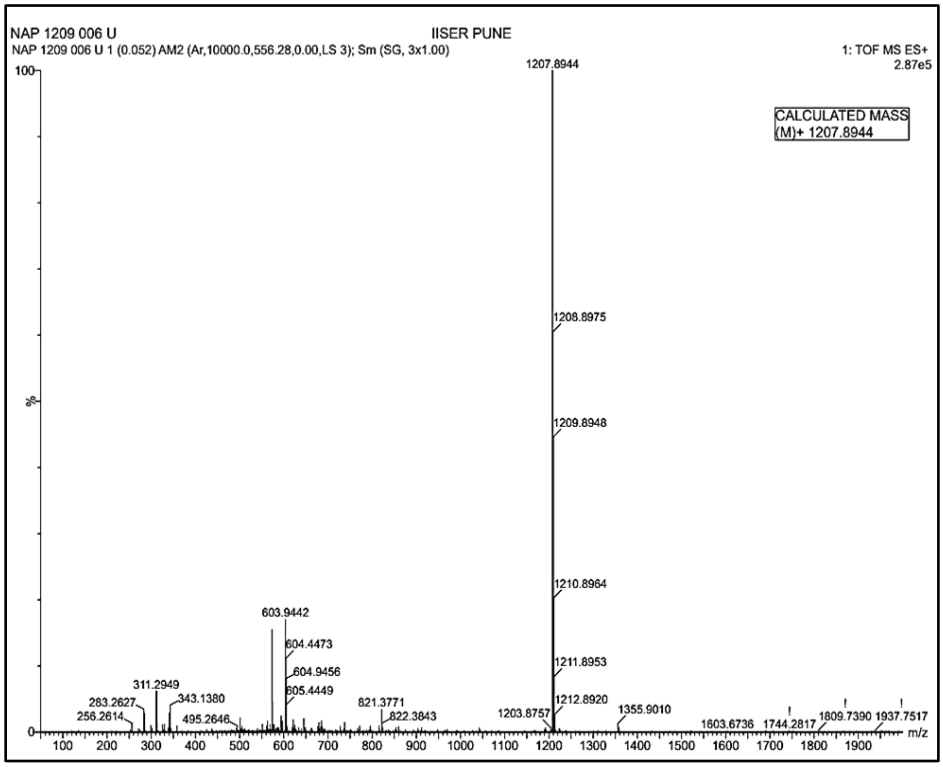

Figure-16: High Resolution Mass Spectrum of **21**.

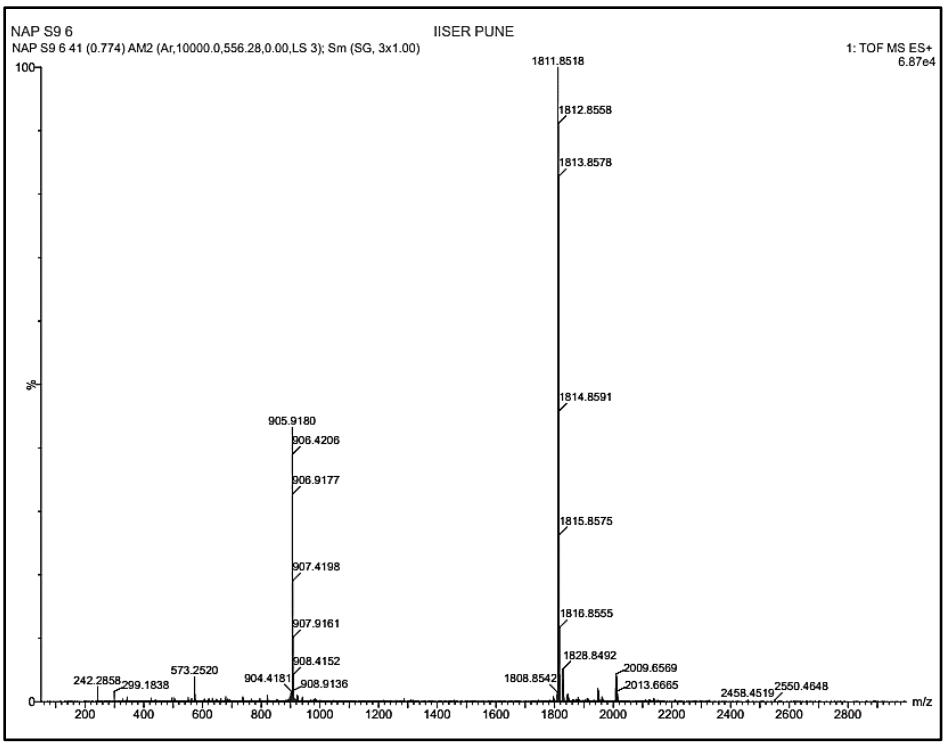

Figure-17: High Resolution Mass Spectrum of **22**.

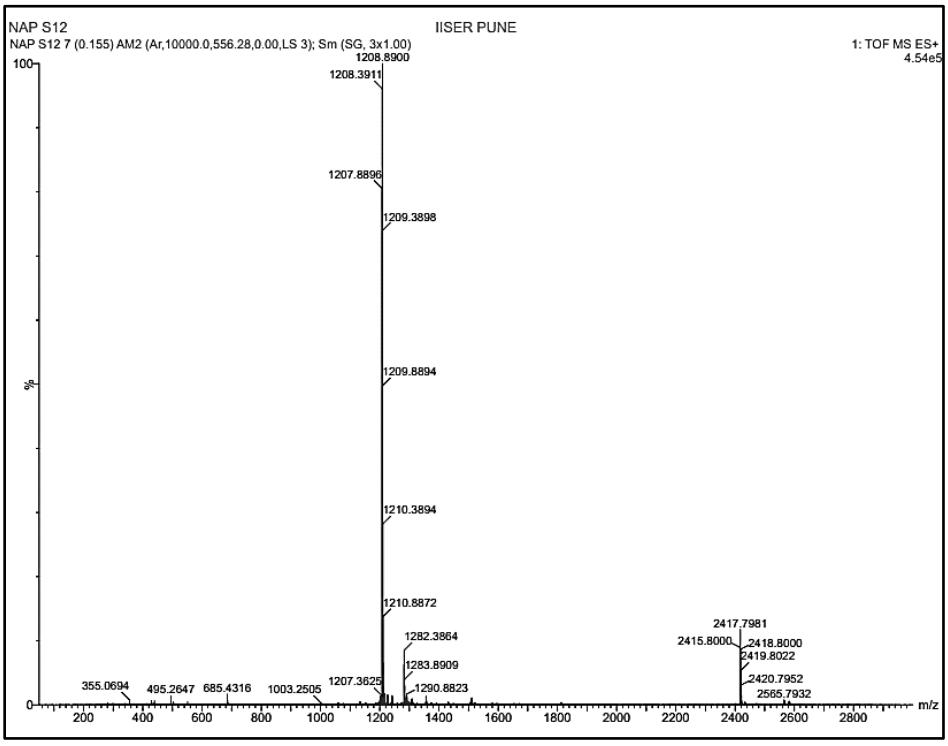

Figure-18: High Resolution Mass Spectrum of **23**.

3.2 NMR CHARACTERIZATION

All the macrocycles characterized by ^{1}H NMR spectroscopy displayed a highly-resolved spectra at RT. Symmetrical nature of all the macrocycles was revealed by ^{1}H NMR studies. For **21**, two doublets at δ 5.45 and 4.92 ppm and a singlet at δ 4.74 ppm with respect to equivalent number of four hydrogens were observed **(Figure- 19)**. Despite **21** being a 28π anti-aromatic system, no significant paratropic ring current effects, were observed. For **22**, which is a 42π system, two doublets at δ 7.04 and 6.80 ppm and a singlet at δ 6.73 ppm for equal six hydrogens were observed **(Figure- 20)**. Surprisingly, no significant downfield shift was observed indicative of non-aromatic nature of the macrocycle. While for **23**, which is a 56π system, two doublets at δ 7.11 ppm and 6.82 ppm and a singlet at δ 6.40 ppm for equal eight hydrogens were observed **(Figure- 21)**. ^{1}H-^{1}H COSY NMR spectrum recorded for all the macrocycles in *chloroform-d$_3$* at 298K showed one set of correlation for doublets at i) δ 5.45 and 4.92 ppm for **21 (Appendix, Figure-A.4)** ii) δ 7.04 and 6.80 ppm for **22 (Appendix, Figure-A.5)** and iii) δ 7.11 ppm and 6.82 ppm for **23 (Appendix, Figure-A.6)** confirming the coupling of adjacent β protons of the heterocyclic rings.

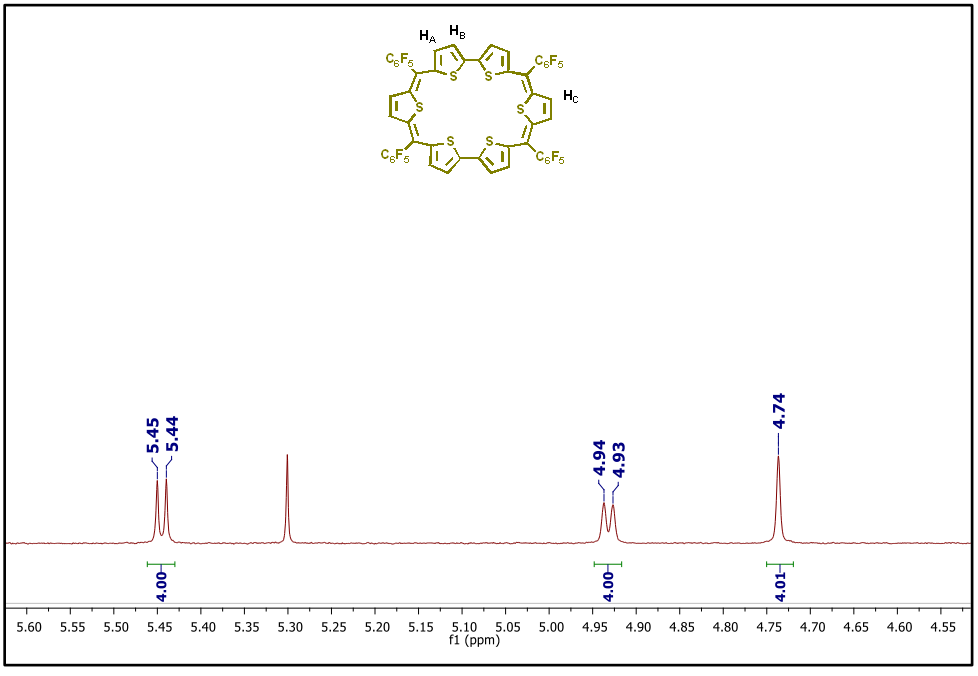

Figure-19: ^{1}H NMR spectrum of **21** in $CDCl_3$ at 298K.

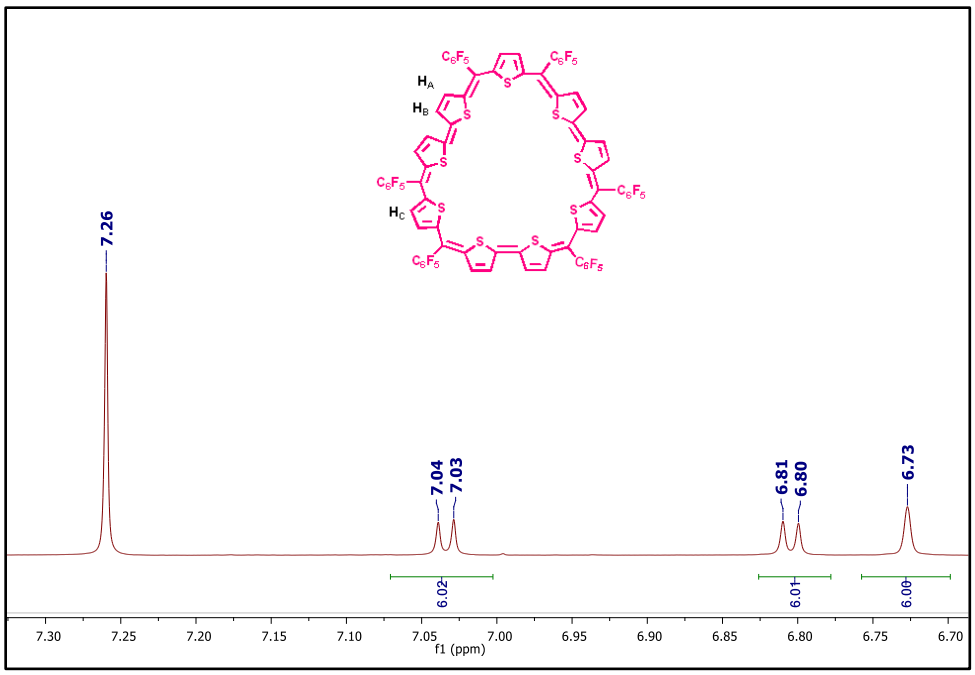

Figure-20: ^{1}H NMR spectrum of **22** in $CDCl_3$ at 298K.

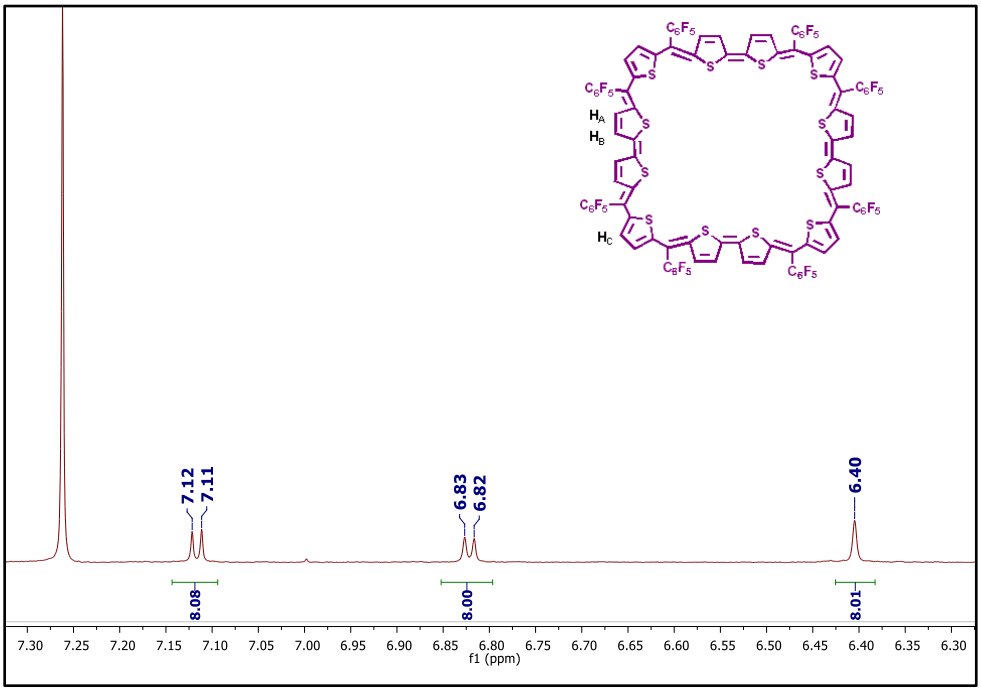

Figure-21: ^{1}H NMR spectrum of **23** in $CDCl_3$ at 298K.

Variable temperature NMR spectroscopy **(Figure-22)** was recorded to arrest the suspected fluxional characteristics of **22**. Upon lowering the temperature, the given signals, i.e., one singlet and two doublets merged into one singlet.

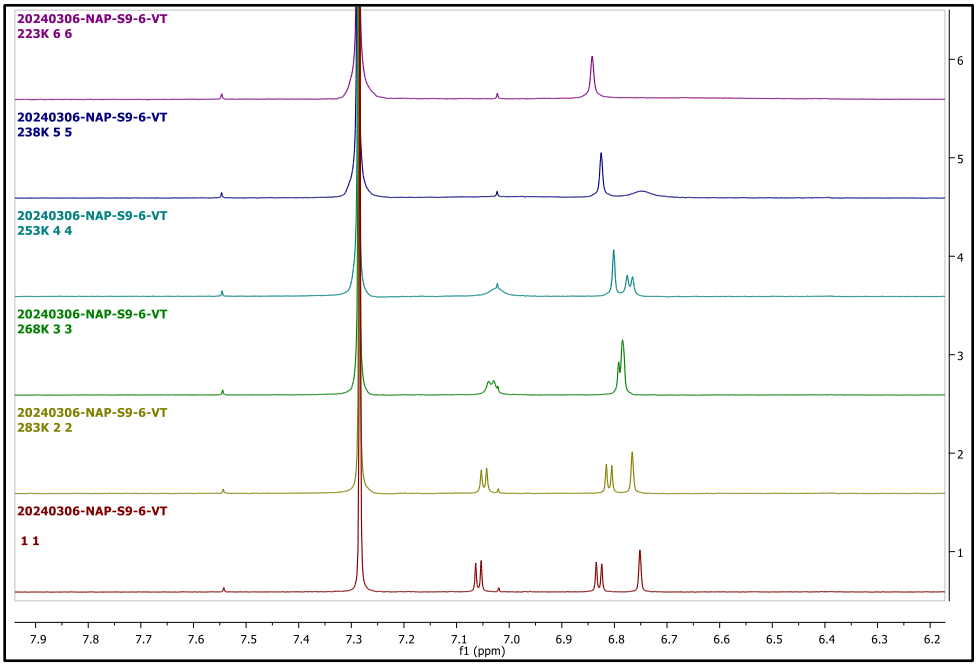

Figure-22: Variable temperature ^{1}H NMR spectrum of **22** in $CDCl_3$ from 298K to 223K.

3.3 UV-VISIBLE ABSORPTION STUDIES

The given macrocycles exhibit color in organic solvents, which absorb in the 400-700 nm range of the electromagnetic spectrum due to extensive π-conjugation. **21** exhibits a pale-yellow color, while **22** and **23** exhibit pink and violet color in dichloromethane respectively. All the three macrocycles were observed to exhibit their absorption in low energy region between 400-600 nm. The λ_{max} was found to be at 454 nm (ϵ=89000 L mol^{-1} cm^{-1}) for **21** while **22** displayed single absorption at 558 nm (ϵ=183000 L mol^{-1} cm^{-1}). Further, **23** displayed absorption at 573 nm (ϵ=176900 L mol^{-1} cm^{-1}). Since large π systems are highly susceptible to oxidations, all the macrocycles were reacted with an oxidizing agent like $[Et_3O]^+[SbCl_6]^-$. They undergo reversible ring oxidation in presence of oxidizing agent. It

was observed that for **21** λ_{max} shifts from 454 nm to 553 nm while it shifts from 558 nm to 778 nm for **22**. **23**, on the other hand displayed a visible red shift from 573 nm to 976 nm. **(Figure-23)** Thus, the red shift of 99nm for **21**, 220 nm for **22** and 403 nm for **23** was accompanied by change in color from yellow to pink for **21**, from pink to blue for **22** and from violet to pink for **23** respectively, as a consequence of oxidation to their respective oxidized states. **(Figure-24)** The red shifted absorption spectra are an indicative feature of an extraordinary shift in the HOMO-LUMO gap.

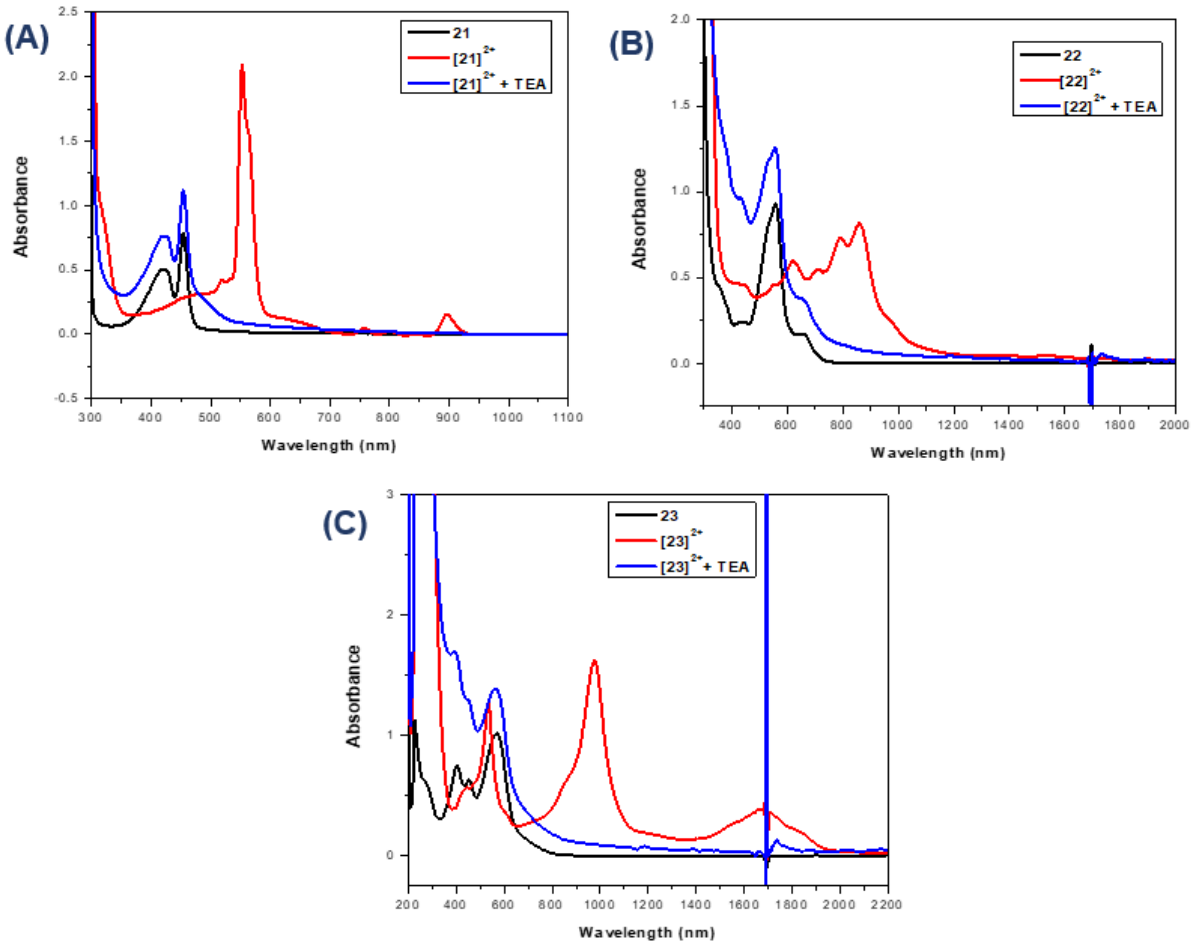

Figure-23: Electronic absorption spectra showing the reversible oxidation of **21 (A)**, **22 (B),** and **23 (C)** in dichloromethane.

Figure-24: Change in color of the given macrocycles to their corresponding dications upon oxidation with Meerwein's salt.

3.4 REDOX PROPERTIES

To analyze the redox behavior of **21, 22** and **23**, Cyclic Voltammetry (CV) and Differential Pulse Voltammetry (DPV) **(Figure-25)** were employed using a three-electrode system- a glassy carbon working electrode, a platinum counter electrode and a calomel reference electrode. The supporting electrolyte was a freshly prepared 0.1M tetrabutylammonium perchlorate (TBAP) solution in dichloromethane. A scan rate of $50mVs^{-1}$ was maintained for all the measurements carried out on CH Instruments Electrochemical Analyzer.

The macrocycle **21** exhibits two oxidation peaks +0.612 V and +0.716 V and a single reduction peak at -0.84 V. Therefore, suitable redox reagents could be employed to oxidize this 28π antiaromatic system to the 26π aromatic state and then further be reduced back to the 28π system. The macrocycle **22**, on the other hand displayed five oxidation peaks at +0.736 V, +1.096 V, +1.324 V, +1.488 V and +1.588 V and four reduction peaks at -1.61 V, -1.34 V, -1.09 V, -0.95 V. The macrocycle **23** displayed three oxidation peaks at +0.62 V, +1.084 V, +1.556 V and three reduction peaks at -1.396 V, 1.28 V and -0.972 V respectively. Therefore, suitable redox reagents could be employed to oxidize the 42π aromatic system (**22**) and the 56π (**23**) antiaromatic system to their respective oxidized systems.

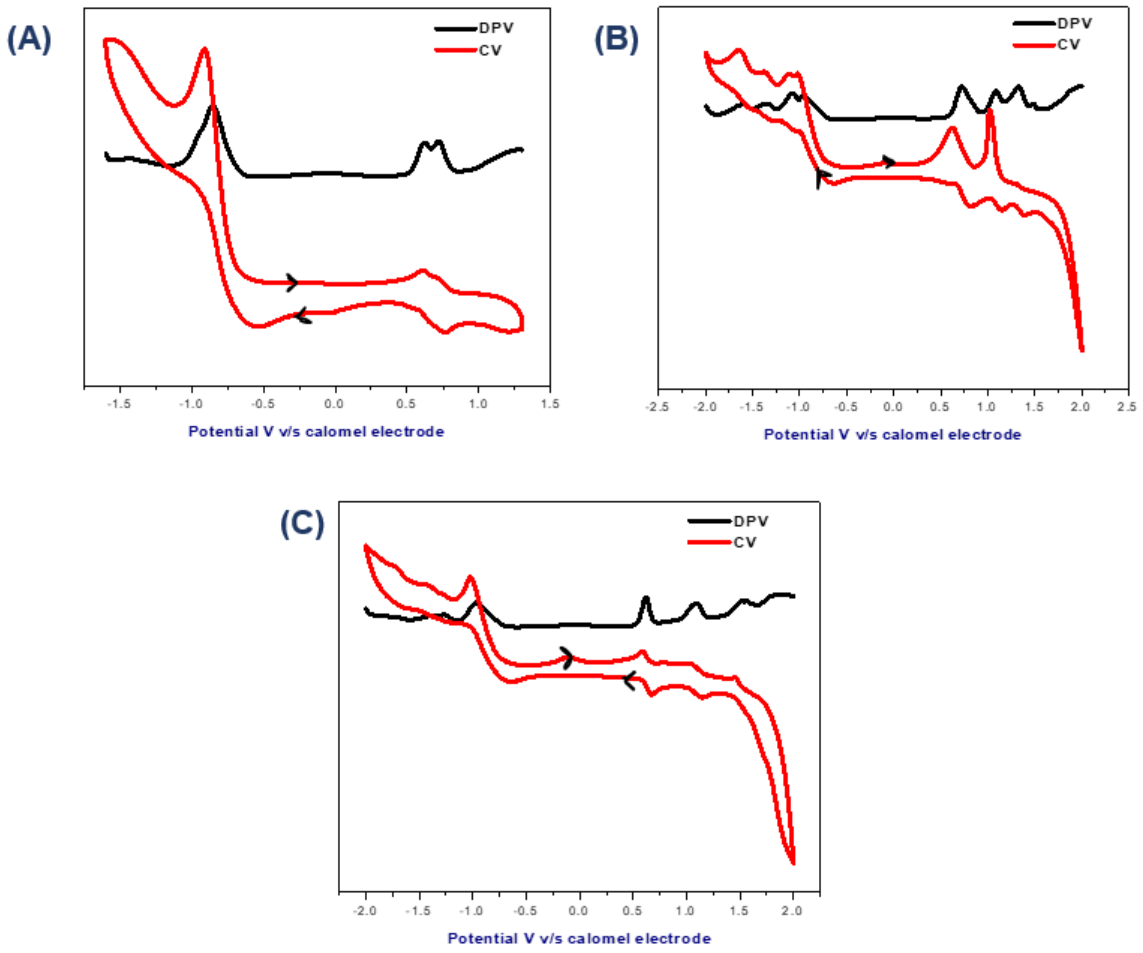

Figure-25: Cyclic (red) and Differential Pulse Voltammogram (black) of Oxidation-Reduction cycle of **21 (A)**, **22 (B)** and **23 (C)** in DCM containing 0.1M TBAP as the supporting electrolyte, recorded at a scan rate of 50mVs^{-1}.

3.5 SPECTRO-ELECTROCHEMISTRY (SEC) STUDIES

The facile reversibility of the two-electron oxidation was confirmed further through SEC studies. All the measurements were carried out in Ocean Insight FLAME Miniature Spectrometer by incorporating the CH Instrument Electrochemical Analyzer in 0.1M TBAP (supporting electrolyte) solution prepared in freshly distilled dichloromethane. Herein, a quartz glass cell (1 mm optical path length), and a three-electrode system (a platinum gauze working, a platinum wire counter and calomel as reference electrode) were

employed. The UV-visible absorption spectra were taken after every 10 seconds. The electronic spectrum of the 28π system, **21**, was recorded at a potential of +0.95 V based on the potential values derived via Cyclic Voltammetry. A wide signal at 518 nm along with a strong signal at 550 nm were seen in its absorption at +0.95 V. The UV-visible absorption spectrum of the 42π system, **22**, recorded at a potential of +1.4 V, displayed two broad peaks at 780 and 850 nm respectively, in support with the UV-Vis absorption spectrum. The 56π system, **23**, on the other hand displayed two peaks at 930 and 970 nm respectively, upon recording the electronic spectrum at +1.7 V **(Figure-26)**.

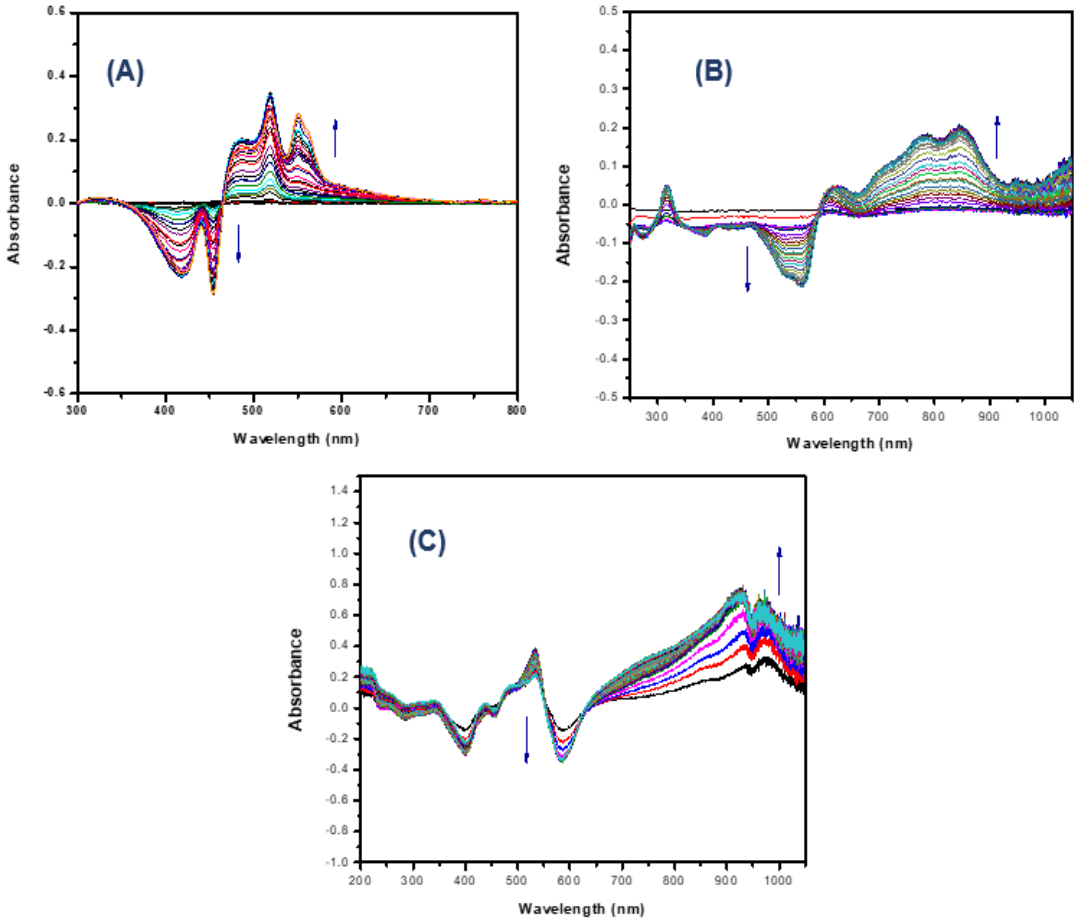

Figure-26: Change in absorption spectra of **21 (A)**, **22 (B)** and **23 (C)** upon an applied potential of +0.95 V, +1.4 V and +1.7 V respectively.

3.6 SINGLE-CRYSTAL X-RAY DIFFRACTION ANALYSIS

The Single-Crystal X-ray diffraction examinations were utilized to discover the molecular structures of **21**, **[21]$^{2+}$** and **22**. Through the gradual evaporation of Hexane into a THF solution of **21**, good quality single-crystals were produced. The solution state structure as established by ^{1}H NMR spectroscopy was validated by the solid-state analysis. Good quality single-crystals of **[21]$^{2+}$** were obtained through the gradual evaporation of n-hexane into acetonitrile solution. A planar geometry was observed for both **21** and its dication. Both showed a rectangular shaped conformation with all the thiophene sulfurs towards the macrocyclic center. Further, by the slow evaporation of Methanol into DCM solution, good quality single crystals of **22** were grown. A planar geometry was observed for **22** with each thiophene of the bithiophene unit pointing away from the macrocyclic core. All our attempts to get good quality single crystals for **23** went futile, despite trying various solvent combinations. However, through geometry and energy optimization, the following conformation **(Figure-30)** was observed as energetically most favorable. Selected crystallographic details are provided in **Table-1**.

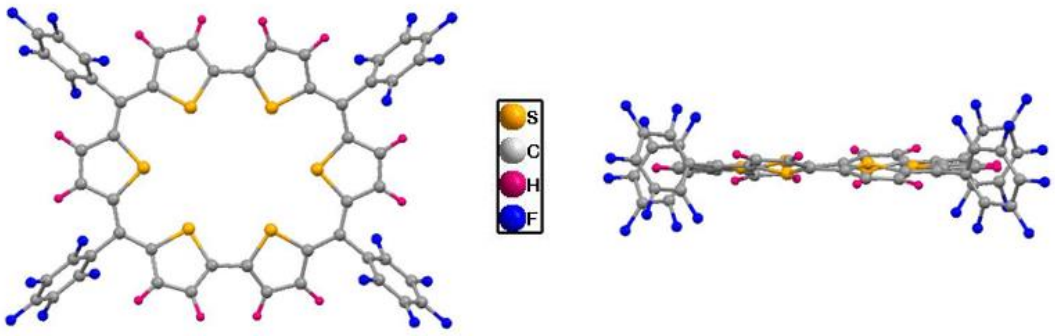

Figure-27: Molecular structure of **21**. Top view (left) and side view (right).

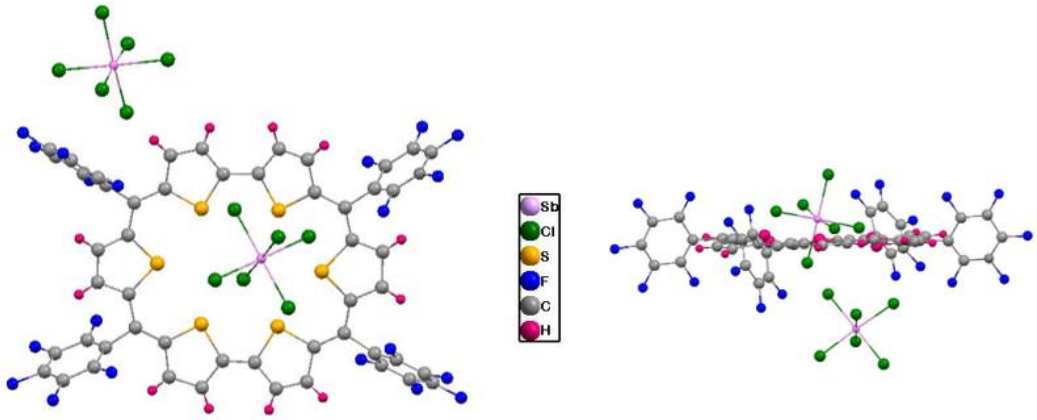

Figure-28: Molecular structure of **[21]**$^{2+}$. Top view (left) and side view (right).

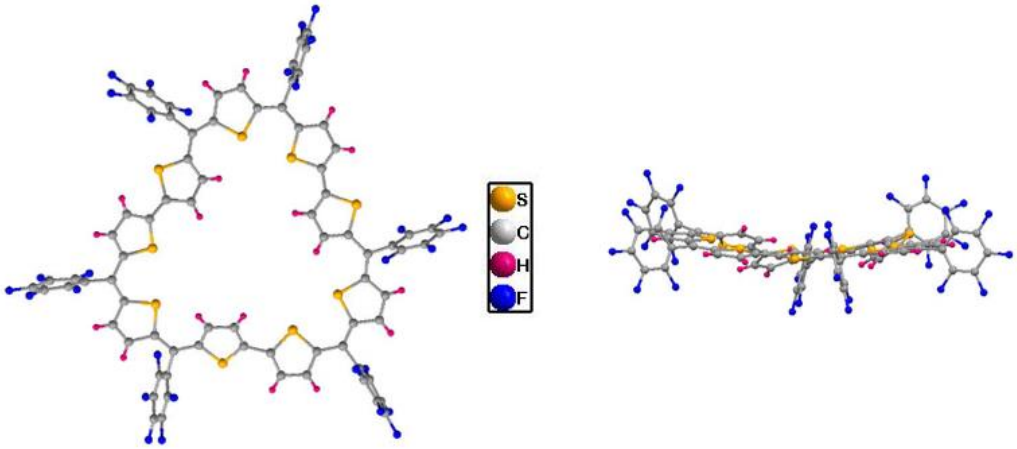

Figure-29: Molecular structure of **22**. Top view (left) and side view (right).

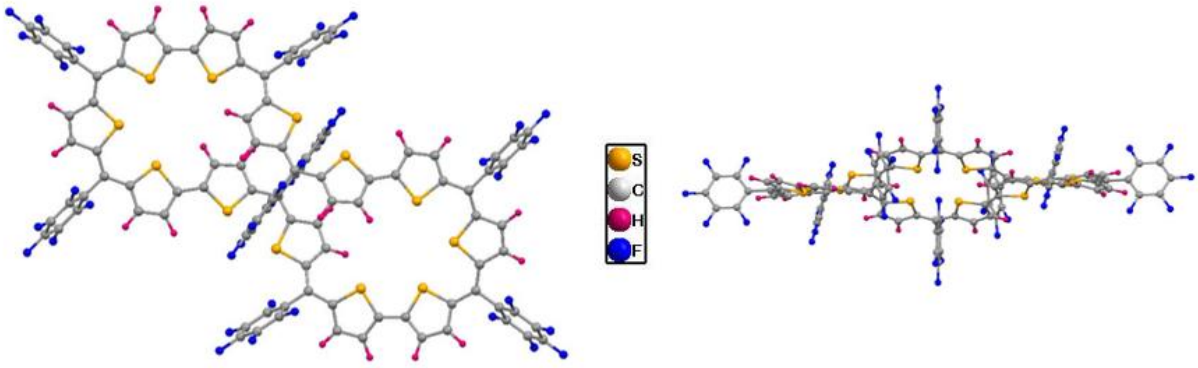

Figure-30: Energy optimized structure of **23** obtained using B3LYP /6-31G(d, p) level of theory in DFT calculation. Top view (left) and side view (right).

Macrocycle	**21**	**[21]$^{2+}$**	**22**
Solvent of crystallization	THF/Hexane	ACN/Hexane	DCM/Methanol
Empirical formula	$C_{52}H_{12}F_{20}S_6$	$C_{52}H_{12}Cl_{12}F_{20}S_6Sb_2$	$C_{78}H_{18}F_{30}S_9$
Temperature (K)	100	100	100
Crystal System	tetragonal	orthorhombic	Monoclinic
Space group	P 4/n c c	P n a 21	C 2/c
Volume	5104	6593	14543
a	11.840	34.964	41.272
b	11.840	12.931	11.169
c	36.408	14.582	31.647
α	90	90	90
β	90	90	94.468
γ	90	90	90
Z	4	4	264
Calculated density	1.651	1.933	1.932
F(000)	2520	3712	8448
Goodness of fit (F^2)	1.383	1.073	1.146
Final R indices {I>2s(I)}	0.0581	0.0600	0.0782

Table-1: Crystallographic data for **21, [21]$^{2+}$, 22**.

3.7 COMPUTATIONAL STUDIES

Gaussian09 program suite [36] along with a High-Performing Computational-Cluster facility at IISER PUNE have been employed for Quantum mechanical calculations. Computational calculations, including Nucleus Independent Chemical Shift (NICS), Anisotropy Induced Current Density (ACID) were performed on the given macrocycles to correlate with the obtained experimental data. Density Functional Theory (DFT) with "Becke's three-parameter hybrid exchange functional, the Lee-Yang-Parr correlation functional (B3LYP), and the 6-31G(d,p) basis set," was used for quantum mechanical calculations using the Gaussian09 software.

3.7.1 Nucleus Independent Chemical Shift (NICS)

The strength of magnetic field determines paratropic or diatropic ring-current effects of the π-conjugated macrocycles, which can be theoretically estimated by NICS calculations. The calculation typically involves i) Geometry optimization, ii) fixing the position of Bq (Banquo or the smallest ionic metal, i.e., Li^+) atom and iii) NMR type calculation using GIAO (Gauge Independent Atomic Orbital) method. The diatropic ring-current of 'aromatic' molecules causes a negative NICS value at the interior position of the ring. Moreover, the effect of paratropic ring-current of 'anti-aromatic' rings typically causes a positive value of NICS. The estimated NICS(0) value for **(21)** is δ +11.20 ppm, while for **(22)** and **(23)** it is δ -2.71 ppm and δ +0.33 ppm respectively **(Table-2)**.

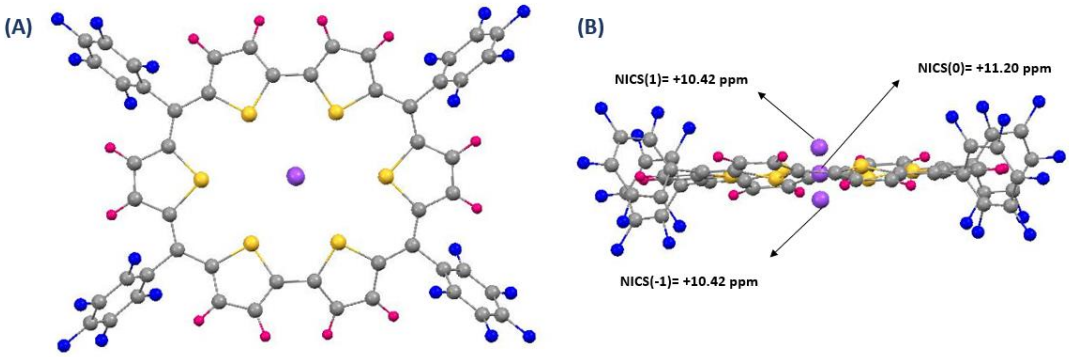

Figure-31: NICS values for **21** calculated using the standard GIAO (NMR=GIAO) at centre of the macrocycle and 1Å above & below the macrocyclic plane along z-axis (a) Top view, (b) Side view.

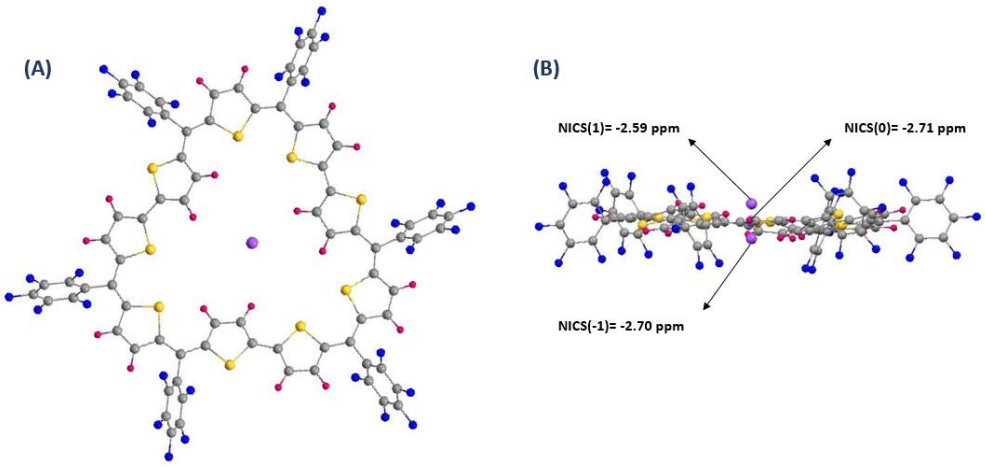

Figure-32: NICS values for **22** calculated using the standard GIAO (NMR=GIAO) at centre of the macrocycle and 1Å above & below the macrocyclic plane along z-axis (a) Top view, (b) Side view.

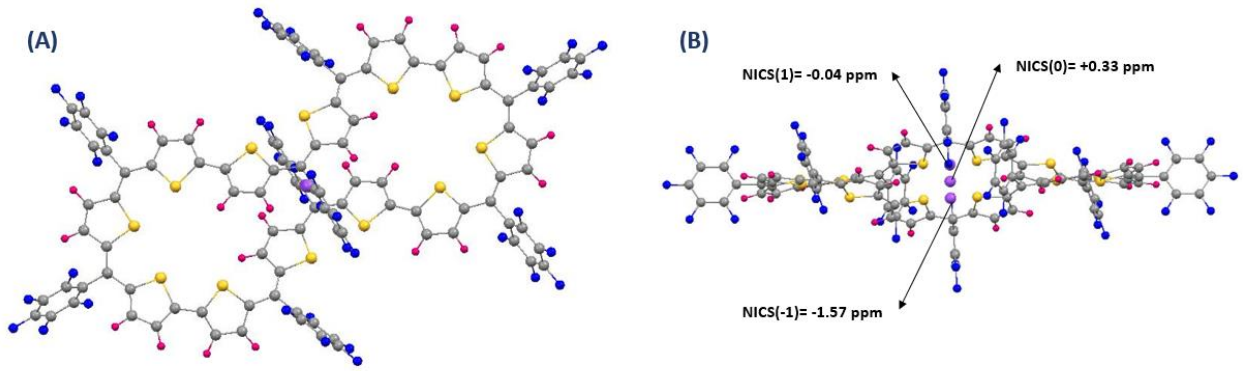

Figure-33: NICS values for **23** calculated using the standard GIAO (NMR=GIAO) at centre of the macrocycle and 1Å above & below the macrocyclic plane along z-axis (a) Top view, (b) Side view.

3.7.2 Anisotropy Induced Current Density (AICD)

ACID, a general method developed by Herges [37] to quantify and visualize the electron delocalization is calculated using the CSGT (Continuous Set of Gauge Transformations) method. These results are plotted in POVRAY 3.7 for Windows. If the π-electron delocalization exhibits a clockwise direction, the given molecule is termed 'aromatic'. On the other hand, if the π-electron delocalization exhibits an anti-clockwise direction, the given molecule is termed 'anti-aromatic'. **(21)** and **(23)** however didn't display anti-clockwise electron delocalization in support of the lack of a significant effect of paratropic

ring-current, as seen in their ^{1}H-NMR spectra while **(22)** didn't display any significant clockwise-direction of electron density, thus confirming its non-aromatic character.

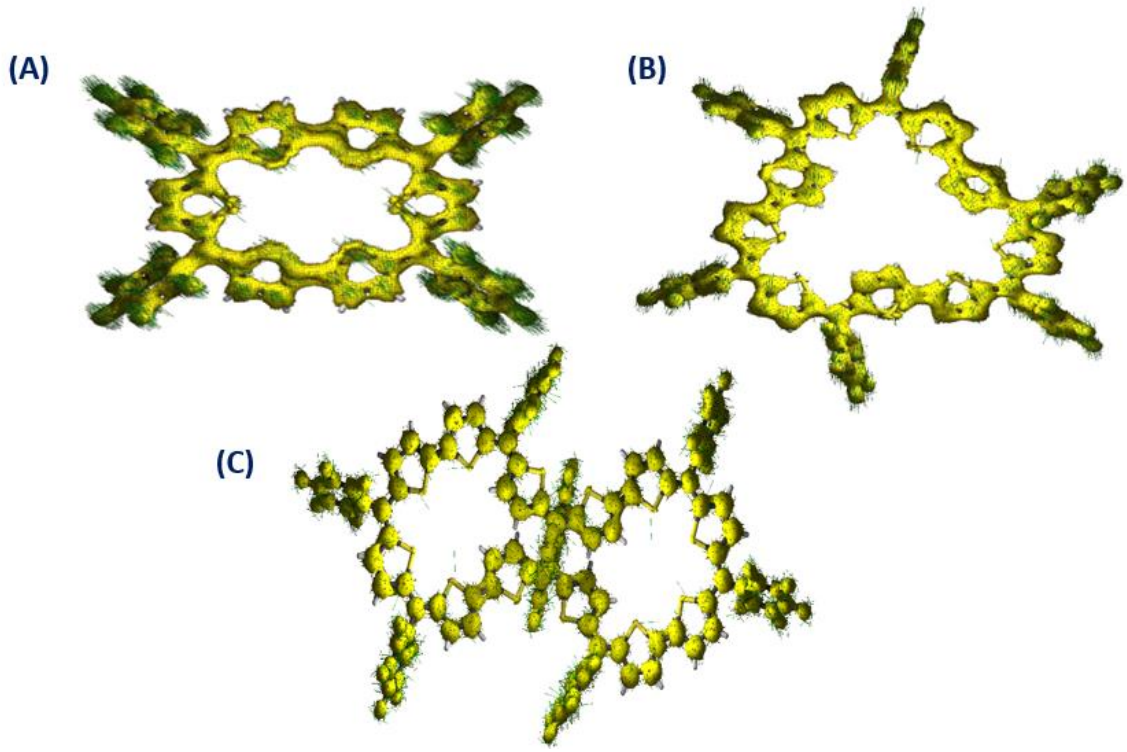

Figure-34: AICD plot of **21 (A), 22 (B)** and **23 (C)** at isovalue 0.06, (π-electrons only) calculated with B3LYP/6-31G(d,p) level of theory.

3.7.3 Singlet-Triplet and HOMO-LUMO Energy Gap

The value of HOMO-LUMO energy gap, by employing B3LYP/6-31G (d,p) basis set was estimated to be 0.78 eV for **(21) (Figure-35)**, 0.92 eV and 0.76 eV for **(22) (Figure-36)** and **(23)** respectively **(Figure-37)**.

Macrocycle	NICS(0) (ppm)	λmax (nm)	HOMO-LUMO (eV)	Huckel Aromaticity
21	+11.20	453	0.78	Anti-aromatic
22	-2.71	558	0.92	Non-aromatic
23	+0.33	573	0.76	Non-aromatic

Table-2: NICS (0) and HOMO-LUMO Energies calculated at B3LYP/6-31G (d) basis set using Gaussian09.

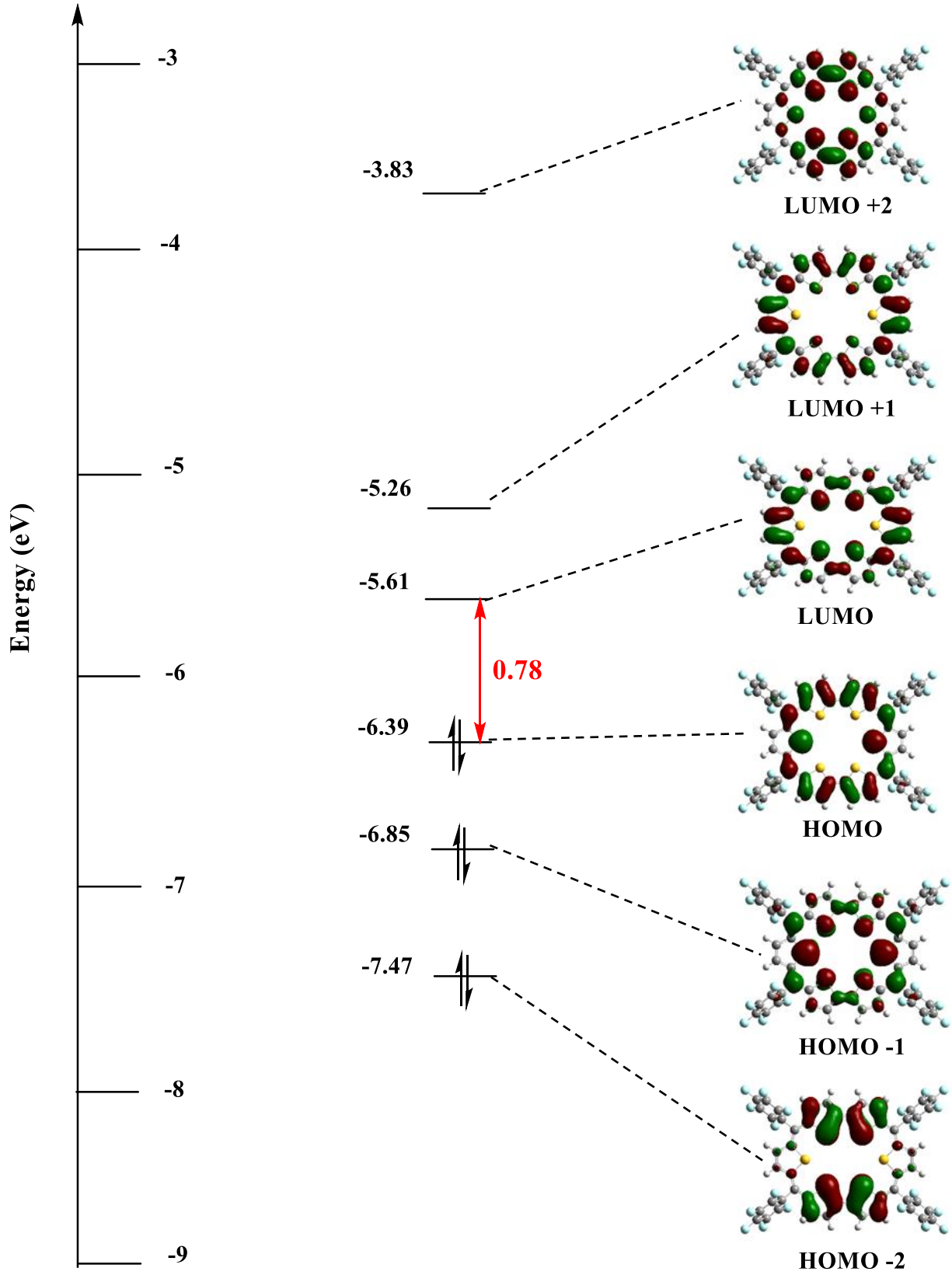

Figure-35: HOMO-LUMO of **21** calculated at the B3LYP/6-31G(d,p) level.

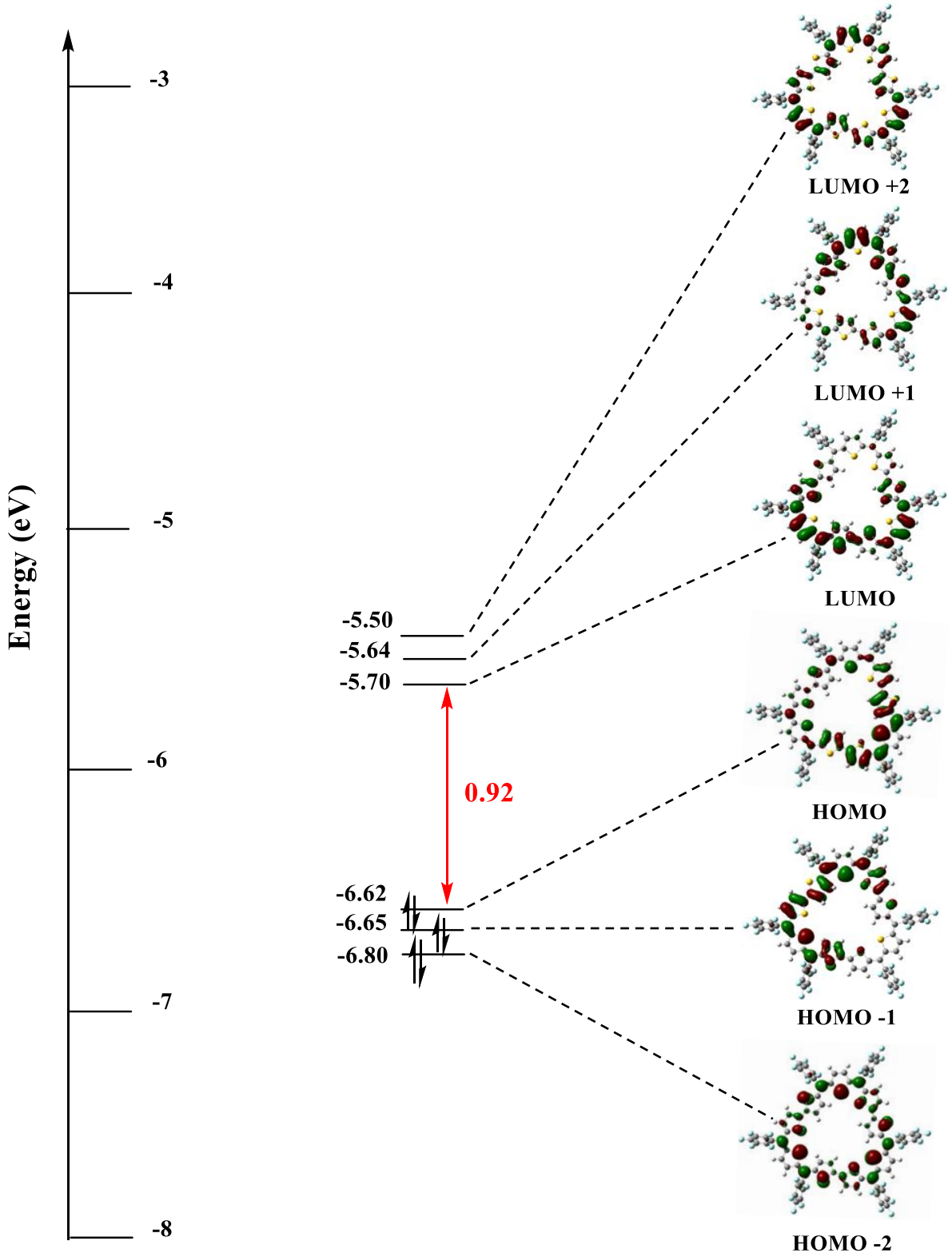

Figure-36: HOMO-LUMO of **22** calculated at the B3LYP/6-31G(d,p) level.

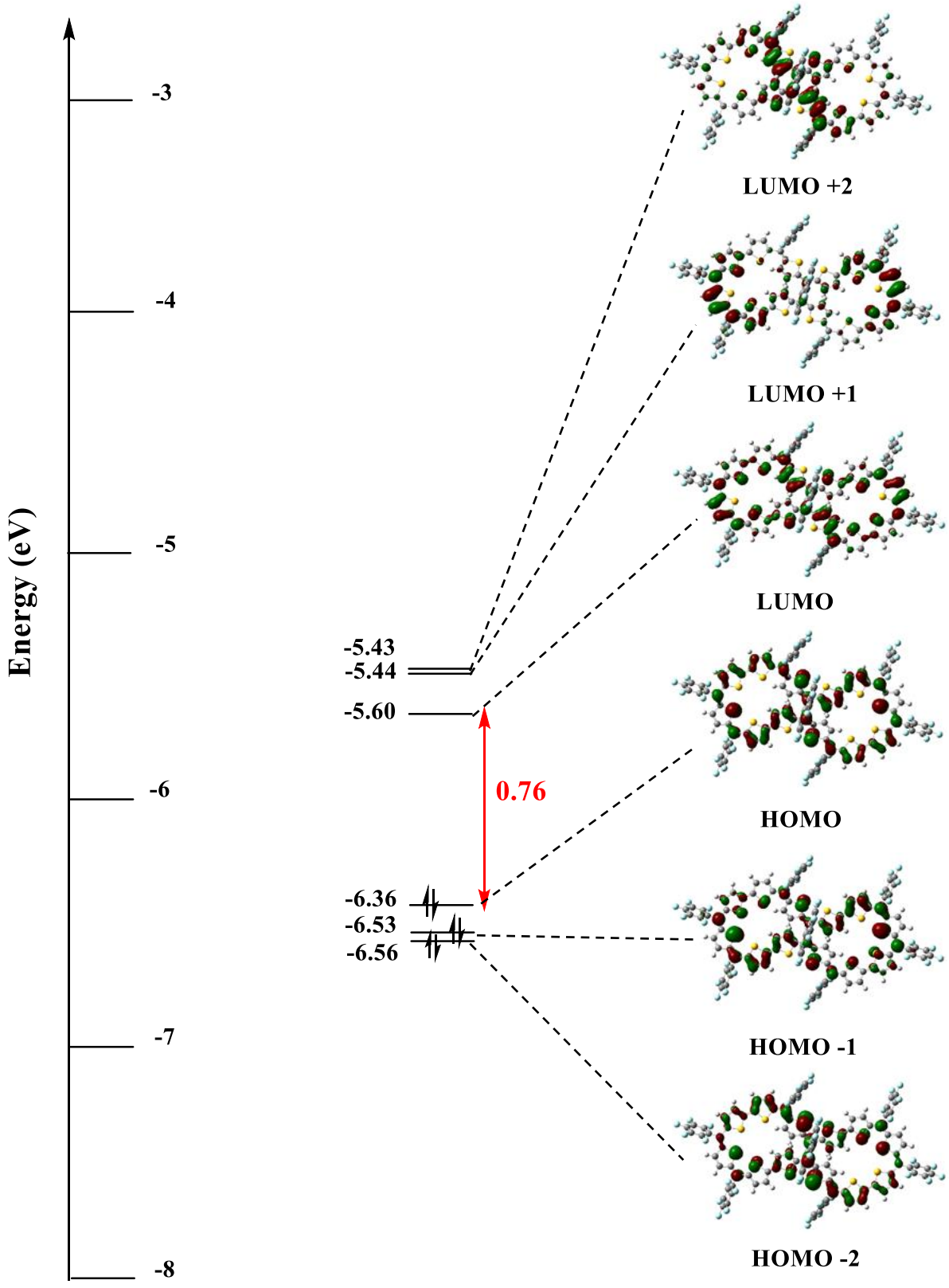

Figure-37: HOMO-LUMO of **23** calculated at the B3LYP/6-31G(d,p) level.

3.8 ESR SPECTROSCOPY STUDIES

An effective cyclic π-conjugation pathway in expanded porphyrins is known to stabilize organic radical species. The low aromaticity of thiophene could be used for the generation of π-conjugated systems.[38] The existence of aromatic diradical states have been known to exist in quinoidal polythiophenes. The presence of a quinoidal bithiophene gives rise to the anticipated diradical character. Upon attaining a benzenoid form, it gains its aromaticity leading to the formation of stable diradical species. The presence of a quinoidal bithiophene unit in the given macrocycles inspired us to investigate the diradical characteristics. The macrocycle **22** was oxidized with the help of Meerwein's salt and further characterized through HRMS. The HRMS (ESI) spectrum displayed *m/z* value of 905.9213 calculated for $[C_{78}H_{18}F_{30}S_9]^{2+}$ $(M)^{2+}$ (905.9208) **(Figure-38)**, thus confirming the oxidation of **22** via two-electrons. Upon oxidation with Meerwein's salt, a color change from pink to blue was observed. Further, red shifted absorbance in the UV-Visible spectra was observed, leading to broad bands at 790 and 850 nm. This observation was additionally supported by Spectroelectrochemical studies, thus suspecting diradicaloid-like features. Moreover, the given dication was unstable in a variety of polar solvents, thus reverting back to its neutral 42π system. In support of this observation as well as the presence of quinoidal bithiophene unit, ESR spectroscopy was employed to validate the diradicaloid like characteristics of **[22]$^{2+}$** experimentally. The ESR spectra recorded at room-temperature **(Figure-39)** and variable-temperature **(Figure-40)** displayed a featureless signal having a *g* value of 2.009 with a half field of 4.1 for **[22]$^{2+}$**. The strength of the ESR signals was found to increase with lowering in temperature, thus confirming the triplet ground state for the given diradicaloid-like species. The presence of a triplet ground state was further confirmed though quantum mechanical calculations, by estimating the Singlet-Triplet energy gap. Δ E(S-T) calculated using unrestricted UCAMB3LYP/6-31G (d,p) was found to be +1.32 kcal/mol, with the triplet state being lower in energy. Further, the oxidation of (4n+2)π **22** to (4nπ) **[22]$^{2+}$** was supported by NICS(0) which was found to be δ +32.27 ppm at the center of the macrocyclic core.

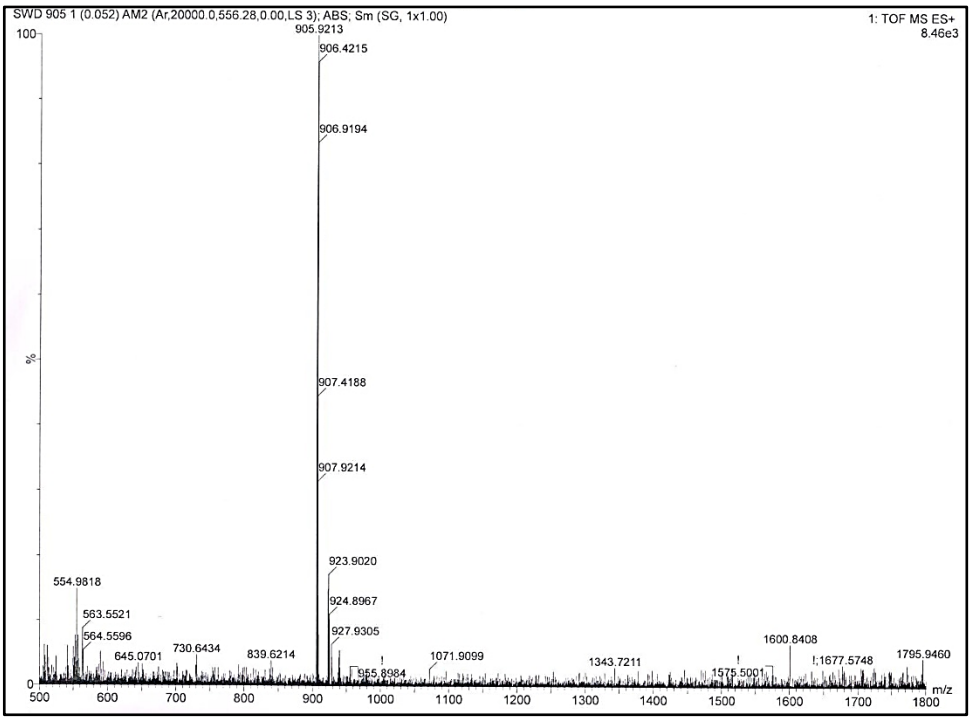

Figure-38: High Resolution Mass Spectrum of **[22]$^{2+}$**.

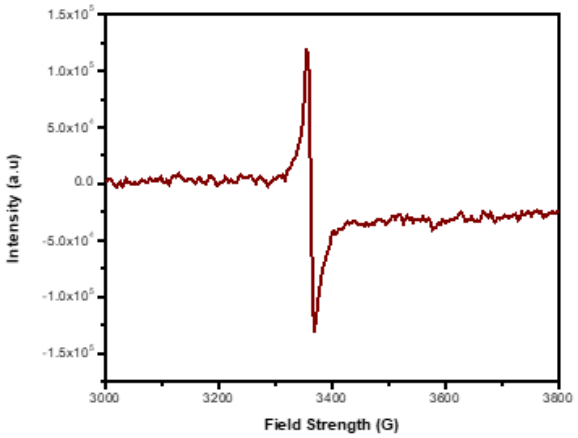

Figure-39: Room temperature EPR spectrum of **[22]$^{2+}$**.

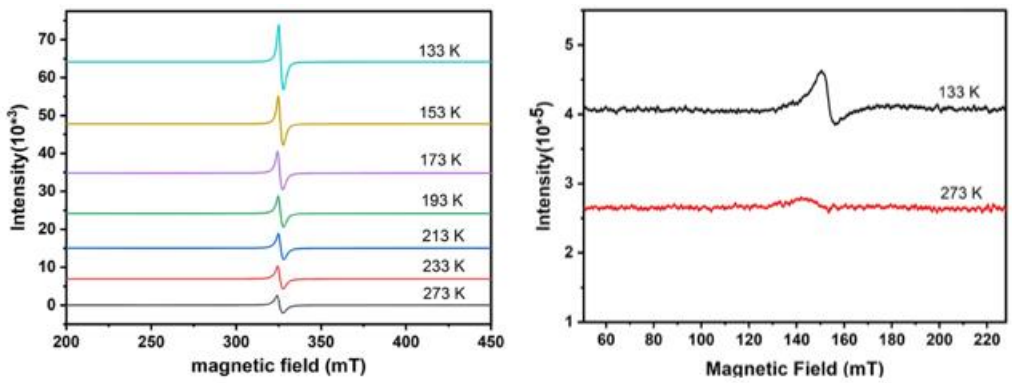

Figure-40: Variable temperature EPR spectra of **[22]$^{2+}$**

CHAPTER-4. DISCUSSIONS

This thesis describes the synthesis, characterization, electronic and redox properties of the given macrocycles. They have been synthesized from simple precursors and characterized through HRMS, ^{1}H-NMR, UV-Visible spectroscopy, Cyclic Voltammetry (CV), Spectroelectrochemistry (SEC), Single-Crystal XRD and Quantum Mechanical calculations respectively.

(21), **(22)** and **(23)** undergo a reversible electron exchange process as seen in the UV-Vis spectroscopy, undergoing red-shifted absorbance. The given macrocycles were subjected to Cyclic Voltammetry and Spectro-electrochemical characterization, in addition to UV-Visible spectroscopy to determine their redox behavior.

Furthermore, the molecular structures of the given macrocycles were determined by growing good quality single crystals in different solvent combinations. While **21** and **22** adopted a planar conformation, the energy-optimized structure of **23** renders it a non-planar conformation.

(21), **(22)** and **(23)** were additionally characterized through Quantum Mechanical calculations, including NICS, and AICD. The AICD plots for all the three macrocycles didn't show any particular direction of electron density and the following observation was also supported by the ^{1}H-NMR spectra and a low value of HOMO-LUMO energy gap of the given macrocycles.

This thesis also covers the diradical chemistry of one of the macrocycles. **[22]$^{2+}$** showed diradicaloid-like characteristics and through experimental and computational characterization, the triplet state was found out to be the lowest energy ground state. The presence of diradical like features in expanded isophlorins can find potential application of these materials in the organic electronics.

APPENDIX

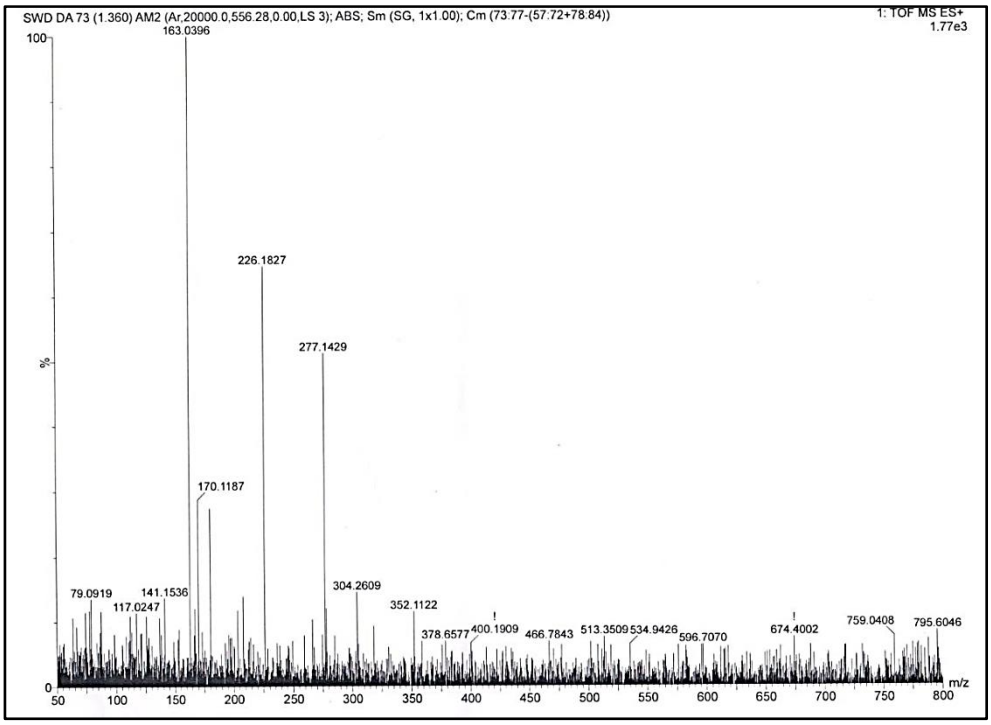

Figure-A.1: High Resolution Mass Spectrum of **17**.

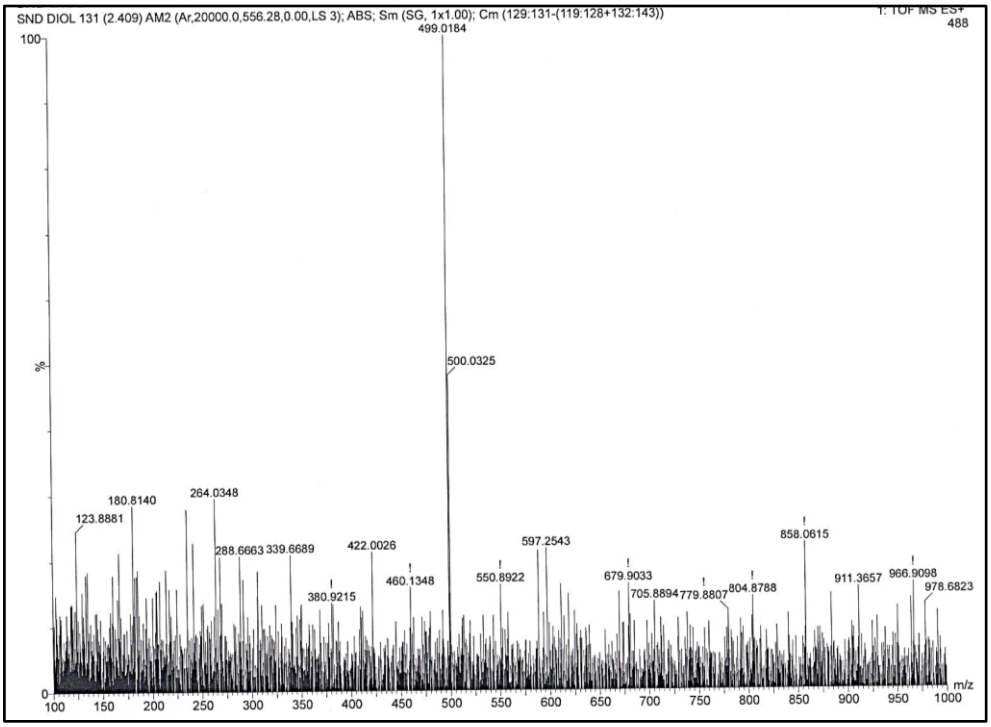

Figure-A.2: High Resolution Mass Spectrum of **18**.

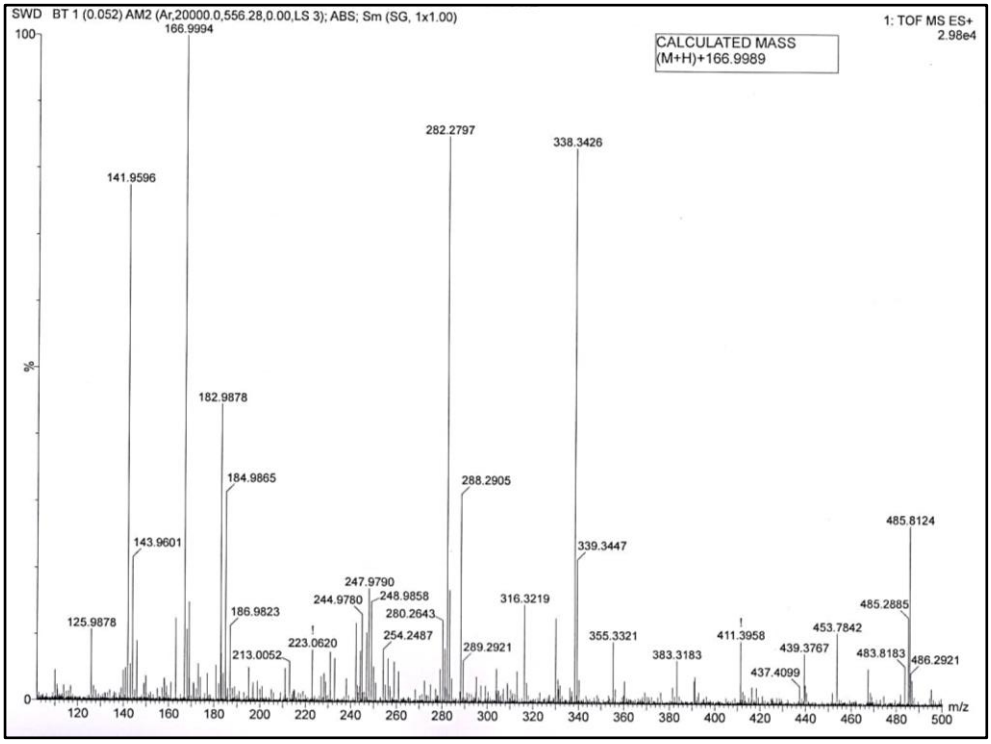

Figure-A.3: High Resolution Mass Spectrum of **20**.

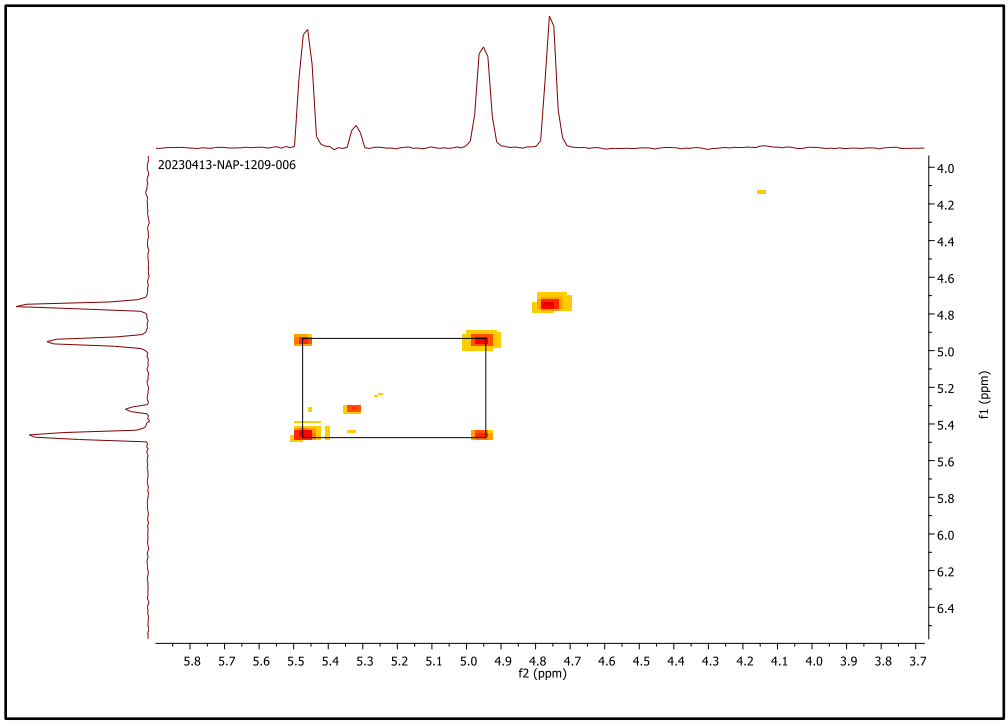

Figure-A.4: ^{1}H-^{1}H COSY 2D NMR of **21**.

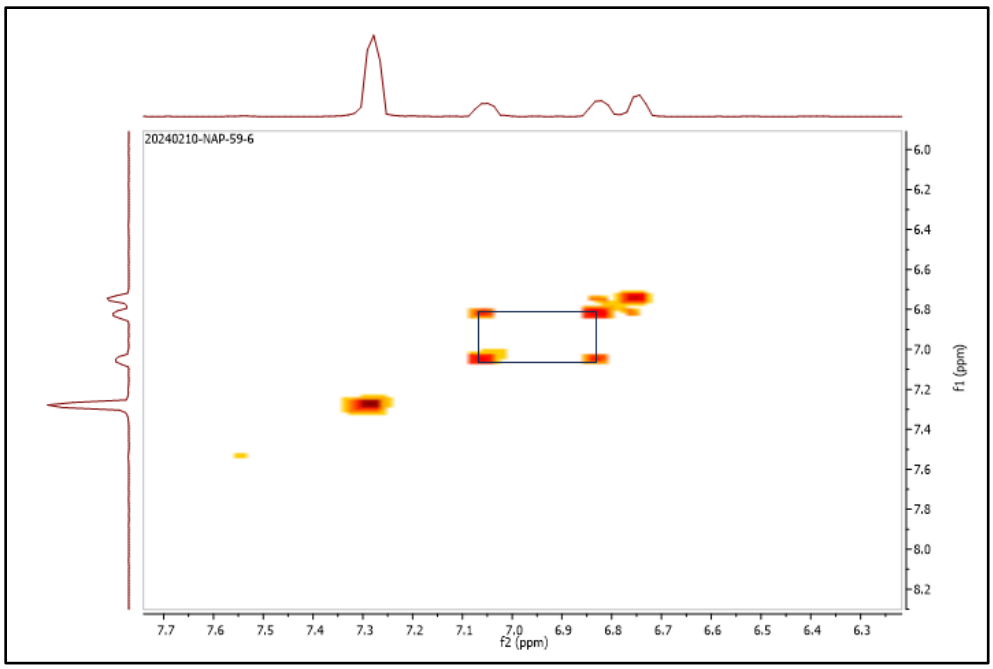

Figure-A.5: ^{1}H-^{1}H COSY 2D NMR of **22**.

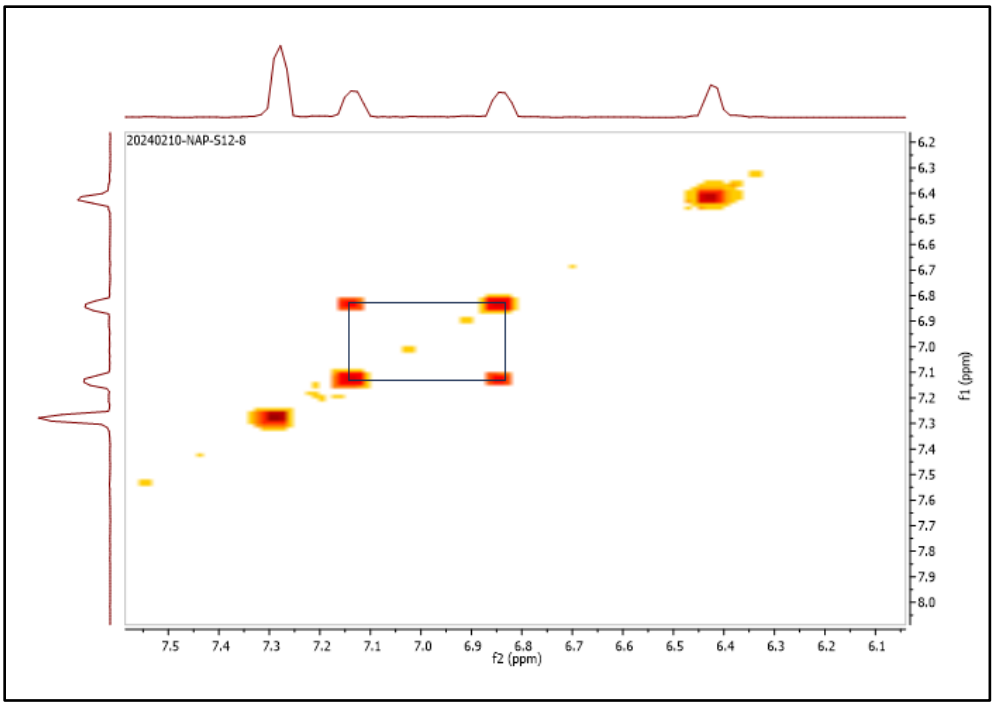

Figure-A.6: ^{1}H-^{1}H COSY 2D NMR of **23**.

REFERENCES

[1] P. J. Garratt, *Aromaticity*, Wiley, New York, **1986**.

[2] a) R. Breslow, *Chem. Eng. News* **1965**, *43*, 90. b) Sondheim.F, *Acc. Chem. Res*. **1972**, *5*, 81. c) R. Breslow, *Acc. Chem. Res*. **1973**, *6*, 393.

[3] (a) For general reviews of the synthesis of annulenes with the emphasis on the work of Sondheimer's group, see Sondheimer, *Proc. Roy. Soc*., **1967**, *A297*, 173. (b) *Proceedings Robert A. Welch Foundation*, XII Organic Synthesis, **1969**, 125. (c) *Pure Appl. Chem*., **1971**, *28*, 331. (d) *Accounts Chem. Res*., **1972**, *5*, 81.

[4]. For 1H NMR spectra of the annulenes see R. C. Haddon, V. R. Haddon and L. M. Jackman, *Top. Curr. Chem*., **1971**, *16*, 103.

[5] R. B. Woodward, *Angew. Chem*. **1960**, *72*, 651.

[6] (a) R. B. Woodward. *Angew. Chem*. **1960**, *72*, 651−662. (b) Y. Yamamoto, Y. Hirata, M. Kodama, T. Yamaguchi, S. Matsukawa, K.-Y. Akiba, D. Hashizume, F. Iwasaki, A. Muranaka, M. Uchiyama, P. Chen, K. M. Kadish and N. Kobayashi, *J. Am. Chem. Soc*., **2010**, *132*, 12627 —12638.

[7] a) E. Vogel, W. Haas, B. Knipp, J. Lex, H. Schmickler, *Angew. Chem. Int. Ed*. **1988**, *27*, 406. b) H. Wilhelm, K. Bernd, S. Martin, L. Johann, V. Emanuel, *Angew. Chem., Int. Ed*. **1988**, *27.* c) E. Vogel, P. Rohrig, M. Sicken, B. Knipp, A. Herrmann, M. Pohl, H. Schmickler, J. Lex, *Angew. Chem., Int. Ed*. **1989**, *28*, 1651. d) M. Pohl, H. Schmickler, J. Lex, E. Vogel, *Angew. Chem., Int. Ed.* **1991**, *30*, 1693. e) R. Bachmann, F. Gerson, G. Gescheidt, E. Vogel, *J. Am. Chem. Soc*. **1992**, *114*, 10855. f) E. Vogel, M. Pohl, A. Herrmann, T. Wiss, C. König, J. Lex, M. Gross, J. P. Gisselbrecht, *Angew. Chem. Int. Ed*. **1996**, *35*, 1520.

[8] a) T. K. Chandrashekar, S. Venkatraman. *Acc. Chem. Res*. **2003**, *36*, 676−691. b) S. Saito, A. Osuka. *Angew. Chem., Int. Ed*. **2011**, *50*, 4342−4373. c) M. Stępien, N. Sprutta, L. Latos-Grazynski. *Angew. Chem., Int. Ed*. **2011**, *50*, 4288−4340. d) J. Y. Shin, K. S. Kim,

M. C. Yoon, J. M. Lim, Z. S. Yoon, A. Osuka, D. Kim. *Chem. Soc. Rev*. **2010**, *39*, 2751−2767.

[9] Pohl, M.; Schmickler, H.; Lex, J.; Vogel, E. Isophlorins: Molecules at the Crossroads of Porphyrin and Annulene Chemistry. *Angew. Chem., Int. Ed. Engl*. **1991**, *30*, 1693-1697.

[10] P. J. Garratt, *Aromaticity*, Wiley, New York, **1986**.

[11] a) R. Breslow, *Chem. Eng. News.* **1965**, *43*, 90; b) F. Sondheim. *Acc. Chem. Res*. **1972**, *5*, 81.

[12] a) E. Vogel, W. Haas, B. Knipp, J. Lex, H. Schmickler, *Angew. Chem. Int. Ed*. **1988**, *27*, 406. b) H. Wilhelm, K. Bernd, S. Martin, L. Johann, V. Emanuel, *Angew. Chem., Int. Ed*. **1988**, *27*. c) E. Vogel, P. Rohrig, M. Sicken, B. Knipp, A. Herrmann, M. Pohl, H. Schmickler, J. Lex, *Angew. Chem., Int. Ed*. **1989**, *28*, 1651. d) M. Pohl, H. Schmickler, J. Lex, E. Vogel, *Angew. Chem., Int. Ed*. **1991**, *30*, 1693. e) R. Bachmann, F. Gerson, G. Gescheidt, E. Vogel, *J. Am. Chem. Soc*. **1992**, *114*, 10855. f) E. Vogel, M. Pohl, A. Herrmann, T. Wiss, C. König, J. Lex, M. Gross, J. P. Gisselbrecht, *Angew. Chem. Int. Ed*. **1996**, *35*, 1520.

[13] H. Wilhelm, K. Bernd, S. Martin, L. Johann, V. Emanuel, *Angew. Chem., Int. Ed*. **1988**, *27.*

[14] J. A. Cissell, T. P. Vaid, A. L. Rheingold, *J. Am. Chem. Soc*. **2005**, *127*, 12212.

[15] C. Liu, D.-M. Shen, Q.-Y. Chen, *J. Am. Chem. Soc*. **2007**, *129*, 5814.

[16] E. Vogel, P. Rohrig, M. Sicken, B. Knipp, A. Herrmann, M. Pohl, H. Schmickler, J. Lex, *Angew. Chem., Int. Ed*. **1989**, *28*, 1651.

[17] M. Pohl, H. Schmickler, J. Lex, E. Vogel, *Angew. Chem., Int. Ed*. **1991**, *30*, 1693.

[18] J. S. Reddy, V. G. Anand, *J. Am. Chem. Soc*. **2008**, *130*, 3718.

[19] M. Kon-no, J. Mack, N. Kobayashi, M. Suenaga, K. Yoza, T. Shinmyozu, *Chem. Eur. J*. **2012**, *18*, 13361.

[20] Gopalakrishna, T. Y.; Reddy, J. S.; Anand, V. G. An Amphoteric Switch to Aromatic and Antiaromatic States of a Neutral Air-Stable 25π Radical. *Angew. Chem., Int. Ed*. **2014**, *53*, 10984−1098.

[21] V. J. Bauer, D. L. J. Clive, D. Dolphin, J. B. Paine, F. L. Harris, M. M. King, J. Loder, S.-W. C Wang, R. B. Woodward, *J. Am. Chem. Soc*. **1983**, *105* ,6429−6436.

[22] J.-Y. Shin, H. Furuta, K. Yoza, S. Igarashi, A. Osuka, *J. Am. Chem. Soc*. **2001**, *123*, 7190.

[23] Sessler, J. L, Morishima, T. Lynch. V., Rubyrin: A New Hexapyrrolic Expanded Porphyrin. *Angew. Chem., Int. Ed*. **1991**, *30(8)*, 977-980.

[24] Sessler, J. L.; Weghorn, S. J.; Morishima, T.; Rosingana, M.; Lynch. V.; Lee, V. Rosarin: a new, easily prepared hexapyrrolic expanded porphyrin. *J. Am. Chem. Soc*. **1992**, *114(21)*, 8306-8307.

[25] Bruckner, C.; D. Sternberg, E.; W. Boyle, R.; Dolphin, D. 5,10- Diphenyltripyrrane, a useful building block for the synthesis of meso-phenyl substituted expanded macrocycles. *Chem. Comm*. **1997**, *17*, 1689-1890.

[26] G. P. M. S. Neves, M.; M. Martins, R.; C. Tome, A.; J. D. Silverstre, A.; M. S. Silva, A.; Felix, V.; A. S. Cavaleiro, J.; G. B. Drew, M. Meso- Substituted Expanded Porphyrins: New and Stable Hexaphyrins. *Chem. Comm*. **1999**, *4*, 385-386.

[27] Setsune, J. I.; Katakami, Y.; Iizuna, N. [48]Dodecaphyrin-(1.0.1.0.1.0.1.0.1.0.1.0) and [64]Hexadecaphyrin-(1.0.1.0.1.0.1.0.1.0.1.0.1.0.1.0): The Largest Cyclopyrroles. *J. Am. Chem. Soc*. **1999**, *121(38)* ,8957-8958.

[28] Shin, J. Y.; Furuta, H.; Yoza, K.; Igarashi, S.; Osuka, A. Meso-Aryl-Substituted Expanded Porphyrins. *J. Am. Chem. Soc*. **2001**, *123(29)*, 7190-7191.

[29] a) Shimizu, S.; Taniguchi, R.; Osuka, A. M*eso*-Aryl-Substituted [26] Hexaphyrin(1.1.0.1.1.0) and [38] Nonaphyrin(1.1.0.1.1.0.1.1.0) from Oxidative Coupling of a Tripyrrane. *Angew. Chem. Int. Ed*. **2005**, *44*, 2225 –2229. b) Shimizu, S.; Cho, W. S.;

Sessler, J. L.; Shinokubo, H.; Osuka, A. Meso Aryl Substituted Rubyrin and its Higher Homologues: Structural Characterization and Chemical Properties. *Chem. Eur. J*. **2008**, *14(9)*, 2668-2678.

[30] Rajeev Kumar, Rajneesh Mishra, T. K. Chandrashekhar. Effect of Meso Aryl Substituents on the Synthesis of Core-Modified Expanded Porphyrins. *Org. Lett.* **2006**, *8, 21*, 4847–4850.

[31] Setsune, J.; Toda, M.; Yoshida, T.; Imamura, K.; Watanabe, K. The Synthesis and Dynamic Structures of Multinuclear Complexes of Large Porphyrinoids Expanded by Phenylene and Thienylene Spacers. *Chem. Eur. J.* **2015**, *21*, 12715-12727.

[32] Hosahalli S. Udaya, Ashokkumar Basavarajappa, Tullimilli Y. Gopalakrishna and Venkataramanarao G. Anand. Topoisomers and Aromaticity of a Redox Active 50π Core-Modified Isophlorinoid. *Chem. Comm*. **2022**, *58*, 13931-13934.

[33] (a) Sheldrick, G. M. Acta Crystallogr., *Sect. A: Found. Crystallogr*. **2008**, *64*, 112-122. (b) Sheldrick, G. M. SHELXL-97, Program for Crystal Structure Solution and Refinement; University of Göttingen: Göttingen, Germany, **1997**.

[34] L. J. Farrugia, *J. Appl. Cryst.* **1999**, *32*, 837-838.

[35] (a) Spek, A. L.; PLATON, A Multipurpose Crystallographic Tool, Utrecht, The Netherlands, 2005; b) V. Sluis, and A. L. *Spek. Acta Crystallogr., Sect. A: Found. Crystallogr.* **1990**, *46*, 194-201.

[36] Frisch, M. J.; et al. Gaussian 09, revision B.01; Gaussian, Inc.: Wallingford, CT, 2009.

[37] D. Geuenich, K. Hess, F. Kohler and R. Herges, *Chem. Rev.*, **2005**, *105*, 3758-3772.

[38] a) Z. Zeng, X. Shi, C. Chi, J. T. L. Navarrete, J. Casado and J. Wu *Chem. Soc. Rev.*, **2015**, *44*, 6578- 6596 b) M. Abe, *Chem. Rev.* **2013**, *113*, 7011−7088.